CEFDA05-1336

Task Title: TW5-TPO-ERGITER: MAGNETIC PERTURBATION FOR ELM SUPPRESSION IN ITER

INTRODUCTION

The objective of the task was to finalize the design studies for optimum set of coils generating Resonant Magnetic Perturbations (RMPs) for Type I ELMs control in ITER [1], [2], [3], [4], [5]. This study was strongly motivated by experimental success of Type I ELMs control on DIII-D using external perturbation generated by in-vessel coils with *n=3* toroidal symmetry [6] and lately on JET using *n=1* perturbation from external Error Field Correction Coils (EFCC) [7]. During the period a large number of possible designs of external or in-vessel coils for ITER were analyzed for the reference scenarios (H-mode-q95=3, Hybrid-q95=4 and Steady-state-q95=5) taking into account physical, technical and spatial constraints [4], [5]. The level of stochasticity (Chirikov parameter ~1 at $\psi^{1/2}$~0.95) generated by the I-coils in the DIII-D experiments on ELMs suppression were taken as a reference [6]. Designs with a toroidal symmetry *n=3* was considered to avoid lower *n* numbers *(n=1, n=2)* that produce larger central islands, a potential trigger of central MHD. For example, *n=1* RMPs at certain amplitude triggered lock modes JET [7]. The current needed in RMP coils to ergodize the edge increase with *n* but higher *n* could be also used in principle (however coils currents are usually limited by technical reasons), since the core MHD thresholds usually increases with *n.*

The optimum spectrum of RMPs (small core perturbations and maximal edge perturbations) for all reference scenarios can be generated by coils situated as close as possible to plasma. However, at present the general consensus is that the in-vessel coils should be avoided because of the severe technical constraints and modifications needed for this design. Here we present two designs with very similar characteristics with respect to the edge ergodicity and core perturbations:

1) The 36 external coils on TF coils at 300-200kAt,

2) The 9 mid-plane plug ports coils 150kAt.

In all the estimations given here there is no margin compared to DIII-D reference case and the self-consistent plasma response is not taken into account, hence for vacuum fields.

However the analytical estimations of the screening effect due to the plasma rotation predicted small effect in the pedestal where we want RMPs to be effective, in contrast with the core, where the perturbations are estimated almost an order of magnitude smaller compared to the vacuum fields. This central screening by toroidal rotation is a positive effect that would reduce a risk of triggering core MHD.

2006 ACTIVITIES

NUMERICAL METHODS

In this section we give a short summary of the methods developed for the task to model RMP spectrum and estimate the plasma edge ergodisation [1], [5]. The RMPs coils are represented schematically by zero-thickness wires in 3D space. Assuming the plasma magnetic response to be very small, the perturbation magnetic field is calculated as if in vacuum using Biot and Savart formula in cylindrical coordinates (*R,ø,Z*). A poloidal spectrum of the radial magnetic perturbation is calculated in the intrinsic flux coordinates: (s,θ,ϕ). Here $s=\sqrt{\psi}\in[0,1]$ is a normalized radial coordinate, ψ is the normalised poloidal magnetic flux, *ø* is the toroidal angle and the poloidal angle θ is defined such that $\frac{d\phi}{d\theta}=-q(\psi)$ -a safety factor.

The magnetic equilibrium is calculated using the HELENA code. The perpendicular to the magnetic surface ("radial") component can be represented as $B^{(1)}\approx(\vec{B}_{eq},\vec{\nabla}s)$, where $\vec{B}_{eq}=\vec{\nabla}\phi\times\vec{\nabla}\psi+F\vec{\nabla}\phi$ and $F(\psi)=RB^{\phi}$ is the product of the major radius R and the toroidal magnetic field B^{ϕ}. Notice, that in the equilibrium case without RMPs $B_{eq}^{(1)}=0$. In order to obtain a physical normalized radial component one should use the formula: $b^{(ph)}=(\vec{B}_{eq},\vec{\nabla}s)/(B_{eq}\sqrt{g^{11}})$, where $g^{11}\equiv(\vec{\nabla}s,\vec{\nabla}s)$. The radial component can be presented as a sum over poloidal and toroidal harmonics: $B^{(1)}(s,\theta,\phi)=\sum_{n=-\infty}^{\infty}\sum_{m=-\infty}^{\infty}B_{mn}^{(1)}(s)e^{i(m\theta+n\phi)}$

To estimate the island size and the degree of overlapping of the edge islands and hence the edge ergodisation, Poincaré plots were obtained by integrating the field-line equations. However, for a quantitative and more rapid estimation of the level of ergodicity the cylindrical approximation for island width and Chirikov parameter has proven to be rather efficient since its results are very close to direct field-lines integration. Introducing the effective radial coordinate *r=as* (where *a* is the minor radius) as a mark for the magnetic surfaces, defining the effective radial coordinate vector as: $\vec{e}_r=\vec{\nabla}s/<g^{11}>_{\theta}$ and using the procedure of field lines integration near resonant surface one obtains the expression for the magnetic island half-width:

$\delta_{m,n} \approx \left(4R_0 a q^2 b^r_{res} / (m \frac{dq}{ds}) \right)^{1/2}$, and the distance between the neighbouring surfaces as:

$$\Delta_{m,m+1} \approx a / (n \frac{dq}{ds})$$

The Chirikov parameter $\sigma_{Chir} = (\delta_{m,n} + \delta_{m+1,n}) / \Delta_{m,m+1}$ is a characteristic of the degree of overlapping for islands. Here the amplitude of the effective radial perturbation normalised to the magnetic field on the axis is calculated as:

$$b^r_{res} \; \left| 2B^1_{mn} \right| / (B_0 < g^{11} >_\theta)$$

Note that at fixed b^r_{res} and for a given *q* profile, σ_{Chir} scales as: $(R_0 a)^{1/2} / a \sim \varepsilon^{-1/2}$.

The reference level of ergodisation needed for ELMs suppression was taken from the experiment on DIII-D [6]. The ITER-like (in terms of triangularity and elongation) configuration with optimum pumping was taken from the shot DIII-D#125913 (R_0=1.72m, $<\delta>$~0.5, κ=1.78, B_0=1.9T, I_p=1.55MA, q_{95}=3.5, where Type I ELMs were suppressed by I_{coil}=4kA (at even parity). The time traces of this shot are presented on figure 1.

The main effect of the RMPs is the density control, leading to the small decrease of the total pressure gradient and hence, to the edge MHD stabilization, in particular pressure gradient driven ballooning-peeling modes responsible for Type I ELMs.

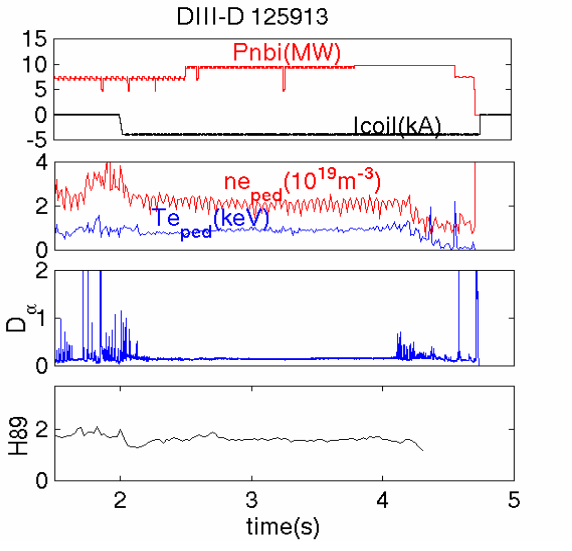

Figure 1: Time traces of reference shot of DIII-D with Type I ELMs suppression by RMPs generated by I-coils at constant confinement. From the top to the bottom:
(a) Neutral beam power and coil current
(b) Pedestal electron temperature and density
(c)-Da signal
(d) Confinement factor

A schematic view of I-coils on DIII-D (a), poloidal spectrum of RMPs (b) and estimated islands size(c) are presented on figure 2 for DIII-D reference shot 125913.

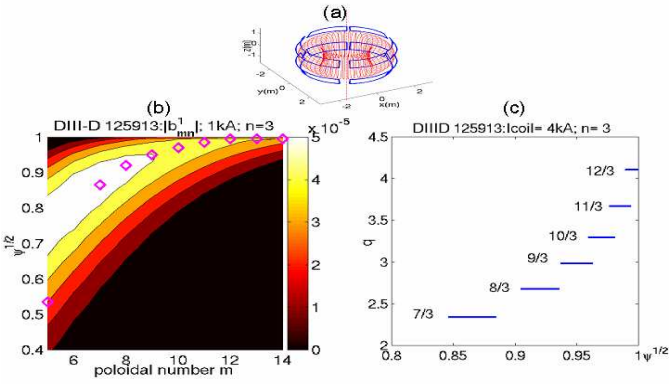

Figure 2: A schematic view of I-coils on DIII-D (a), poloidal spectrum of RMPs with the position of resonant surfaces (diamonds) (b); islands position and width (c) for DIII-D reference shot 125913. The ergodic region where islands overlap starts at $\psi^{1/2}$>0.95, hence Chirikov parameter >1

DESIGNS OF RMP COILS FOR ITER

The aim of the design work for ITER was to propose the coils system and phasing between coils in a way that edge resonant surfaces *q=-m/n* (signs of *m* and *n* are conventional, but opposite since *q>0*) are situated near the maximum of the spectrum that is the case on figure 2(b) for DIII-D. However, notice that the RMPs spectrum is specific for each equilibrium and in particular q-profile through the pitch angles of the field lines as they pass in front of the RMP coils. As a consequence, in design studies for ITER the variation of equilibrium for different reference scenarios (H-mode- q95=3, Hybrid q95=4, and Steady-state q95=5) were analyzed. Also the changes in equilibrium due to the changes in internal inductance (li), βp, edge magnetic shear in the reasonable range for ITER scenarios were done but demonstrated to have small effect on the edge ergodisation.

Because of the rapid decrease of the magnetic perturbation with the distance from the coils the RMP coils the optimum case would be coils situated as close as possible to plasma.

However, due to the strong technical restrictions for the in-vessel implantation in ITER, external coil designs were considered initially as the more feasible option. After studies of the available space in ITER the realistic geometrical parameters were taken into account. Here we propose the best design of external coils (18 upper and 18 lower fixed close to TF coils shown on figure 3) found up to now that require ~300kAt to obtain the same ergodisity for all ITER reference scenarios considered here.

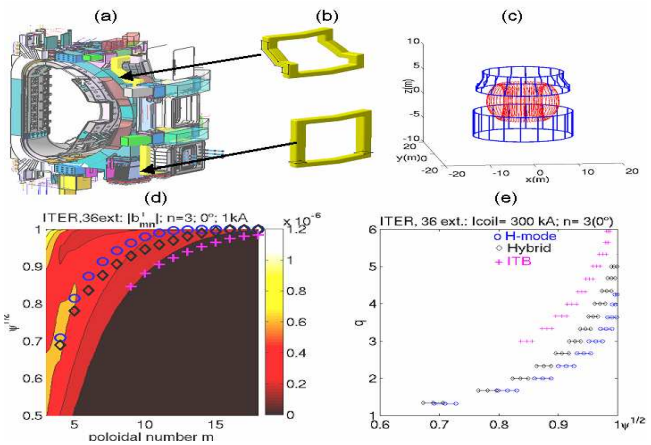

Figure 3: A schematic view of 36 external RMP coils (a,b,c) ,RMPpoloidal spectrum for n=3 (d) and island size(e) for three ITER scenarios. The ergodic region where islands overlap: $\psi^{1/2}$>0.95, hence Chirikov parameter >1

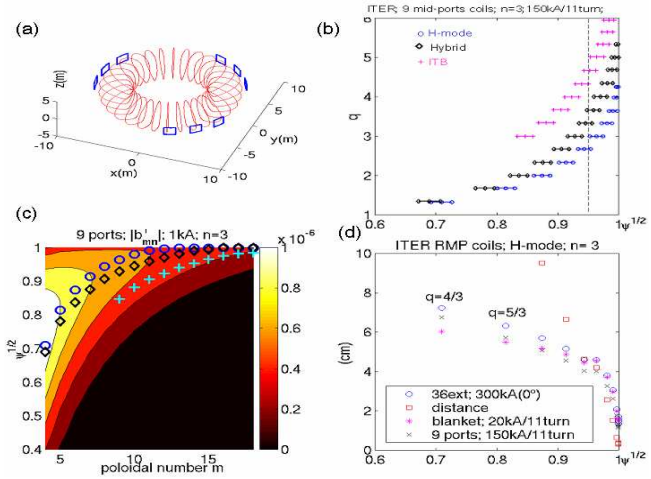

Figure 4: A schematic view (a) of the first turn of the mid-port coils (each coil is represented by 11 turns wired from R=8.7m to 9.2m), RMP poloidal spectrum (c) and island size for 150kAt (b) for three ITER scenarios. (d)-comparative island size calculated in vacuum for reference H-mode equilibrium (li=0.8, βp=0.6) for three designs included 36 external coils(300kAt), 9 ports coils(150kAt) and 6 upper and 6 lower in-vessel coils(20kAt) around the blanket modules [3]

Similar characteristics for mid-ports design are presented in figure 4. Here we took into account the fact that not all ports are available (only 9 from 18 ports were used here) because of the heating systems installed in them. From the figure 4(d) one can see that central (q=4/3) island size estimated for vacuum increases only slightly from 6cm for in-vessel coils to 8cm for more external coils, but edge ergodisation is similar for these three designs, hence one can avoid in-vessel coils.

In all the estimations given here there is no margin and the self-consistent plasma response is not taken into account, hence for vacuum fields. The changes in equilibrium due to the changes in internal inductance (li), βp, edge magnetic shear in the reasonable range for ITER scenarios were studied and were demonstrated to have small effect on the edge ergodisation. These results are not presented here. The most strong plasma response on RMPs however, is due to the plasma rotation.

It was shown in [3] that the radial component of the vacuum magnetic field in cylindrical approximation on the resonance surface $q=-m/n$ is shielded by plasma rotation:

$$B_{m,n}^{r,pl} = \frac{B_{m,n}^{r,vac}}{\sqrt{1+(\Omega\tau_L/2/m)^2}} = S_{fac} B_{m,n}^{r,vac} .$$

Here $\Omega=2\pi n f$ is local toroidal rotation frequency for the mode n, τ_L is the visco-resistive layer time: $\tau_L = 2(\sqrt{1+2q^2}\tau_A)^{2/3}\tau_\eta^{2/3}/\tau_v^{1/3}$, $\tau_A = R/V_A \cdot 1/(n\cdot Sh)$ is the Alfvén time, $Sh = r/q(dq/dr)$ is the local magnetic shear, $\tau_\eta = \mu_0 r^2/\eta$ is the resistive time , $r=a\psi^{1/2}$ is an equivalent radius of the resonant magnetic surface in cylindrical approximation, η is the parallel plasma resistivity, $\tau_v = r^2\rho/\mu$ the viscous time (here we take μ/ρ~$1m^2/s$). The analytical estimations [4] of the screening effect due to the plasma rotation predicted small effect in the pedestal, in contrast with the core, where the perturbations are estimated almost an order of magnitude smaller compared to the vacuum fields (figure 5), which is a positive effect that would reduce the risk of triggering core MHD.

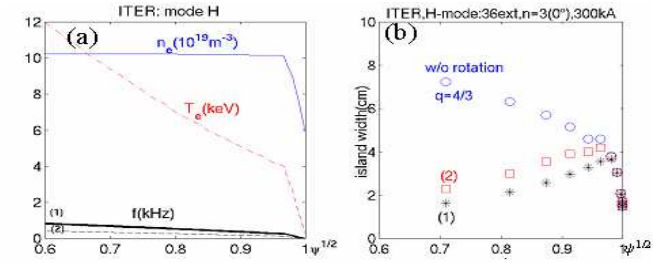

*Figure 5: (a): H-mode scenario profiles used in modelling: electron density(ne), temperature (Te)and two profiles of toroidal rotation f -(1) and (2) which is (1)*0.5, (b): island width for 36external coils design at 300kA ,n=3, without rotation (circus) and with rotation profile (1)-stars, with profile (2)-squares*

REPORTS AND PUBLICATIONS

[1] M. Bécoulet, et al., "Comparative Modeling of Type I ELM control by stochastic fields in DIII-D, JET and ITER", Proc. 32nd EPS Conf. Plasma Physics, Tarragona (2005) P2.005

[2] E. Nardon et al., to be published in J. Nuc Mater (2007)

[3] M. Becoulet et al., "Modelling of Edge Control by Ergodic Fields in DIII-D, JET and ITER", 21st IAEA Conference, Chengdu, China, 16-22 October, 2006, IT/P1-29

[4] Becoulet et al. First Intermediate Report on the Task: TW5-TPO-ERGITER: Resonant Magnetic Perturbations (RMPs) for ELMs suppression in ITER. Design studies of RMPs coils for ITER. CEA/DRFC: PEFC/NTT-2006.016

[5] Becoulet et al, Second Intermediate Report on the Task: CEFDA05-1336 TW5-TPO-ERGITER: Resonant Magnetic Perturbations (RMPs) for ELMs suppression in ITER. Design studies of RMPs coils for ITER. Rep. CEA/DRFC: PHY/NTT-2006.007

[6] T.E. Evans, R.A. Moyer, J.G. Watkins, T.H. Osborne, P.R. Thomas, M. Becoulet, et al, Nuclear Fusion, 45 (2005) 595

[7] Y. Liang, M. Becoulet, E. Nardon et al submitted PRL(2007)

TASK LEADER

Marina BECOULET

DSM/DRFC/SIPP
CEA-Cadarache
F-13108 Saint-Paul-lez-Durance Cedex

Tel. : 33 4 42 25 74 84
Fax : 33 4 42 25 49 90

e-mail : marina.becoulet@cea.fr

TW5-TPO-CODACGW

Task Title: REVIEW OF ITER CONTROL AND DATA ACQUISITION (CODAC) SYSTEM

INTRODUCTION

The objective of this task is to provide support to the review of the ITER CODAC specifications, in particular drawing on experience in the development of the Tore Supra control and data acquisition system.

This task has been launched at the end of January 2006. Since then the working group has met twice in Garching (March) and in JET (May). Meetings have also taken place on separate issues in various places. An interactive web site has been set up with UKAEA support for the people to communicate their work.

2006 ACTIVITIES

Our Association has provided support to the review of the ITER CODAC since beginning of 2006. The Euratom-CEA representative in the working group, participated to the three meetings of the working group.

For the review work we proposed to concentrate its activity on two important issues for the CODAC:
- The CODAC architecture and design feature
- Pulse control and operation.

For the first activity our Association identified manpower and expertise to collaborate with the experts of other associations.

For the second activity detailed discussions have taken place at the European level between in particular CEA, IPP and UKAEA specialists, on the organisation of the operation, the pulse schedule and the editor. This work should come up with a synthesis of a conceptual study during the first half of 2007.

In addition Euratom-CEA formed a pool of specialists to review the main documents of the review, namely: the overview, the list of systems, the design documents and the work-package document. In this pool Euratom-CEA also called for the assistance of specialist of fission reactor operation and safety. These expertises are considered as an essential template for the operation of a fusion reactor.

Our Association has reviewed the overview in April 2006 and given comments and recommendation to the working group. More recently the list of systems has also been reviewed and commented.

There are also some areas where our Association developed a recognised expertise which can be directly applicable to the CODAC review. These areas are:

- Data archiving and structure and data access,
- Software methodology and tools,
- Remote operation control room and communication and standard,
- Synchronous databus and event distribution network,
- Physical networks.

The conceptual study of some of these areas, have made good progress in particular on the communication and standard and on the synchronous databus.

In addition, because of its particular role of host for ITER, the Euratom-CEA Association could facilitate the interaction between the safety issues and the CODAC revision. For this reason we organized a specific meeting between the people in charge of the safety case and the chairman of the working group (J. Lister), in May 2006. This meeting was important to identify the area of interaction between the CODAC and the safety case. During his visit to Cadarache, J. Lister had also the opportunity to detail the on-going work to Euratom-CEA experts. This meeting has been fruitful in identifying the areas where our Association's participation could be optimized.

CONCLUSIONS

The Euratom-CEA Association will continue in the second phase to commit itself in this work and participate to the CODAC revision in the areas described above.

TASK LEADER

Emmanuel JOFFRIN

DSM/DRFC/STEP
CEA-Cadarache
F-13108 Saint-Paul-Lez-Durance Cedex

Tel : 33 4 42 25
Fax : 33 4 42 25

e-mail : emmanuel.joffrin@cea.fr

CEFDA05-1329

Task Title: TW6-TPHI-ICFS: FARADAY SHIELD MODELLING AND RF SHEATH DISSIPATION

INTRODUCTION

The Faraday shield on the ITER ion cyclotron antenna is a critical component: it is the main plasma-facing component for the antenna and must withstand the same heat loads and disruption effects as the first wall; it shields the inner parts of the antenna from particles; it polarizes the IC wave and prevents the electrostatic field on the current strap from coupling to the plasma.

Experiments on Tore Supra and elsewhere indicate that parts of the antenna structure (e.g., guard limiters) can be heated anomalously in the presence of RF fields and plasma; the standard explanation is that RF-induced sheaths and/or convective cells enhance particle and power transport to these regions, thereby causing the observed high heat load. Considerable modeling of this effect has been done in the past. Can a model of these effects be developed and applied to the Faraday shield design for ITER, and what guidance regarding shield geometry can be obtained from these models?

According to specifications the task includes the following activities:

5.2.1) Use RF electric field maps developed as a part of task TW6-TPHI-ICFS, static magnetic equilibria supplied by the IT, and current or improved sheath theories to compute the power lost to RF sheaths in different ITER antenna/Faraday shield configurations. Use density profiles in the scrape-off region, supplied by the IT, corresponding to those used to calculate antenna loading for Scenario 4.

5.2.2) Calculate power deposition profiles on the antenna and surrounding regions for different cases of antenna and Faraday shield geometry. Evaluate the advantages and disadvantages of various geometries, including in particular the case of horizontal and tilted Faraday shield elements, transparent vs. opaque shields and no shield at all for comparison. Consider in particular the case where the antenna is contained completely in a mid-plane port, with the front surface of the Faraday shield being ~ 1 cm behind the first wall.

2006 ACTIVITIES

PRINCIPLE OF RF SHEATH EVALUATION

RF sheath rectification processes can be briefly summarized as follows. ICRF antenna operation drives an oscillating RF potential V_{RF} between the extremities of open magnetic flux tubes, given by $V_{RF} = \int_L E_{//}.dl$, where $E_{//}$ is the RF parallel electric field and integration is along the open field line. As a reaction to this RF potential, and due to the non-linear behaviour of the sheaths at both flux tube extremities, the field line gets biased to a rectified DC potential V_{DC}, which is generally well above typical floating potentials in the Scrape-Off Layer (SOL). Ions accelerated across the high DC potential cause enhanced sputtering and localised high heat fluxes at the field line ends. Moreover the differential biasing of nearby flux tubes creates RF-induced DC **E×B** particle convection transversally to the field lines [3]. The intense RF-induced DC electric fields could also interact with the H-mode [3].
Calculation is thus performed in several steps:

1°) Evaluate $V_{RF} = \int_L E_{//}.dl$ along every open field line, from computed RF field maps.

2°) Evaluate V_{DC} from V_{RF} on each field line. In the simplest RF sheath model, each flux tube is biased independently from its neighbours, to a potential $V_{DC}=|V_{RF}|/\pi$.

3°) Evaluate the density n on each field line. Density is supposed homogeneous along flux tubes so that its determination is a 2D problem transversally to the field lines. Particle transport is due to parallel losses, cross-field diffusion and RF-induced **E×B** convection, and density balance in steady-state regime reads

$$\mathrm{div}\left[-D_{\perp}\nabla n - n\frac{\nabla V_{DC}\times \mathbf{B}_0}{B_0^2}\right] + \frac{nc_s}{L_{//}} = 0 \qquad (1)$$

where $D_{\perp}$ is a particle diffusion coefficient, $L_{//}$ is the length of open field lines, c_s is the sound speed = $[k(T_e+T_i)/m_i]^{1/2}$. The 2D density map needs to be computed only in the region affected by convection. This domain is chosen as a rectangular box. In the radial direction, convective cells penetrate from the antenna mouth up to the point where V_{DC} is of the order of kT_e. From Tore Supra measurements, this is of the order of a few skin depths for the Slow Wave [6]. On the other side it is proposed to stop density calculation at the antenna mouth and not to calculate the density inside the box. This is motivated as follows:

- Geometry is complicated, so that precise boundaries of open field lines are not clear.
- Due to complicated geometry, precision of the local RF field might not be guarantied.
- Connection lengths decrease abruptly inside box, leading to fast density decay.

Equation 1 is solved in the simulation box using the CELLS code [1]. As boundary conditions on the plasma side n is fixed to its "unperturbed value". Density is put at 0 on the antenna side, assuming no recycling from

chamber walls. In the poloidal direction the poloidal derivative of the density is supposed to vanish at the limits of the simulation domain (meaning no poloidal convection).
4°) Evaluate ion parallel heat losses at the extremities of the flux tubes. The particle density outflux is $nL_{//}c_s$ and each ion is accelerated across the sheaths to the energy of eV_{DC}, so that the energy outflux becomes $Q_{//}=enV_{DC}L_{//}c_s$.
5°) Evaluate the transverse heat fluxes at the antenna side. The heat flux is deduced from the particle outflux at the antenna side of the simulation domain, assuming that each particle carries a kinetic energy of the order of kT_e.

PLASMA PARAMETERS

Magnetic equilibrium

The geometry chosen for RF field calculation is a flattened version of the ITER antenna front face. Consistently with this choice a simple magnetic equilibrium is proposed, in which field lines are straight lines parallel to the antenna front face and tilted by a pitch angle of α=15°. The local magnitude of the magnetic field in the antenna vicinity is taken constant at B_0=3.9T, consistently with ITER scenario 2 proposed for computations [7]. Note that since all the geometry is flattened, magnetic field lines are parallel to the antenna front face and no parallel loss is considered on FS rods.

Unperturbed radial profiles

From reference [7], typical SOL radial profiles are available in the zone unaffected by convection. They are shown on figure 1 for ITER scenario 2.

Considerable uncertainty remains on these profiles. This impacts directly on the sheath calculations:
- For given power coupled to the plasma, the magnitude of the RF near fields depends on the antenna coupling resistance, which is quite sensitive to the edge density profile.
- The radial penetration of the slow wave depends on the density at the antenna mouth.
- The local density at the penetration depth roughly determines how many particles are likely to be convected onto the antenna front face.

Extra input parameters needed from IT team

To perform density calculations, typical values of B_0 and T_e and $D_\perp$ in the antenna vicinity need to be provided. As a boundary condition for density computation, the value of the density on the plasma side of the simulation domain needs to be provided.

Typical field line pitch angles in front of antenna are critical since (mis)alignment of antenna structure elements with tilted field lines plays a crucial role in building up the RF potentials.

Radially in front of the antenna structure, open field lines will be supposed to extend over the dimensions of the RF field map, and $E_{//}$ will be taken 0 outside the map. For such field lines $L_{//}$ can be taken as typically $2\pi qR$.

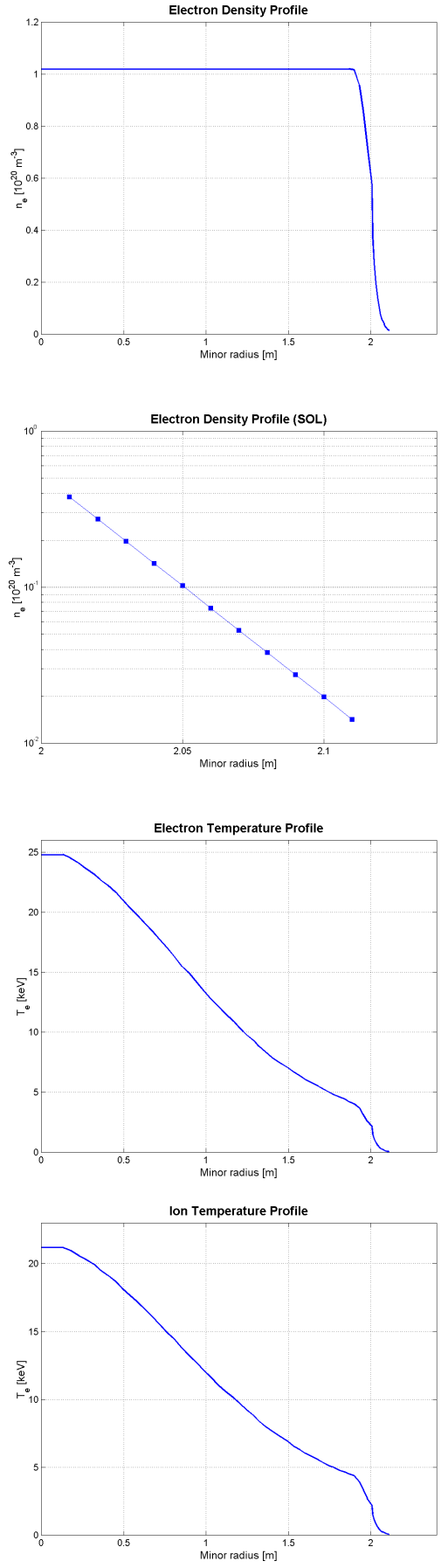

Figure 1: Scenario 2 profiles

RF FIELD MAPS

The first step in the simulation process is a 3D mapping of RF near fields in the antenna vicinity.

Definition of a target medium for RF wave

Antenna code HFSS used in task TW6-TPHI-ICFS cannot handle the most general dielectric tensors of magnetized plasmas. The load used for previous test RF field maps was shown to reproduce fairly well the coupling properties of a typical ITER plasma for the fast wave [4]. However, the present task is mainly interested in parallel RF fields, i.e. the slow wave, whose properties are radically different due to the anisotropy of magnetised plasmas. Slow wave is completely absent of the present HFSS medium, since it is isotropic. Simulations should however preserve realistic coupling to the fast wave, which determines the near field amplitude for given coupled power.

A systematic comparison of uniaxial and gyrotropic homogeneous media was made [9]. From this analysis it appears that part of the information about wave propagation is always lost when approximating gyrotropic with uniaxial media. However there is some latitude in choosing what is lost and what is preserved. Based on these considerations the following fall-back solution was proposed to try to get results using HFSS:

- As in "conventional cases" the domain facing the antenna is composed of a "vacuum zone", followed by an isotropic lossy dielectric where the fast wave is damped.

- In the vacuum zone, transverse dielectric constants are still $\varepsilon_\perp=1$. It is proposed to use a highly negative value for the dielectric constant $\varepsilon_{//}$ parallel to (tilted) magnetic field lines, in order to reproduce the high parallel conductivity in the plasma.

The fall-back solution has the following merits:

- Fast wave propagation, being insensitive to $\varepsilon_{//}$, should not be affected by the change of medium, whatever $k_{//}$.

-For perpendicular propagation $k_{//}=0$, suitable for integrating $E_{//}$ over "long field lines" with large toroidal extension (see [2]) a clear decoupling is possible. Propagation properties of the fast wave depend only on elements S and D of the Stix dielectric tensor, while the squared refractive index for the slow wave takes the form

$$N^2=P \qquad (2)$$

The refractive index for the Slow Wave at $k_{//}=0$ is thus well reproduced when $\varepsilon_{//}=P=1-\omega_{pe}^2/\omega_0^2$. From scenario 2 profiles, P~-24000 at the antenna mouth. For this particular density, the typical evanescence length for the slow wave at $k_{//}=k_y=0$ is typically 6mm. Such rapid decay justifies *a posteriori* the choice of homogeneous plasma parameters near the antenna to represent the Slow Wave. Recent probe measurements on Tore Supra suggest that RF-induced SOL perturbations extend a few centimetres in front of powered antennas, consistently with skin depth estimates [6]. The proposed procedure was never tested previously, and potential drawbacks may arise. The highly anisotropic artificial medium is very demanding for a Finite Element code. The refractive index for the Slow wave is only well reproduced for $k_{//}=0$, whereas other values of $k_{//}$ contribute to the integral of $E_{//}$ over the finite extension of the map. In particular a spurious surface wave is expected for $k_{//}=\varepsilon_\perp=1$, which does not exist in the real plasma when $S<0$. Therefore some basic checks should thus be made on the HFSS results:
- Verify that the input impedance matrix, and particularly its real part, are only weakly affected when $\varepsilon_{//}$ is switched from 1 to –24000.
- Check the radial evanescence of the Slow wave.
- Check the absence of surface wave.

Requirements on RF field maps and antenna structure

Within the simple magnetic equilibrium proposed, only the RF field parallel to tilted straight field lines is needed. Real and imaginary parts $E//$ should be computed, even if the part in phase quadrature with RF currents on the straps is generally dominant. This RF field can be normalized to either 1MW (or 20MW) coupled. The direction of anisotropy in the uniaxial medium should be consistent with the pitch angle $\alpha=15°$. Poloidal and toroidal extension of the map should be such that $E//$ vanishes at map boundaries. This could reveal difficult if surface waves are absent. Tilted field line from map corner should not intersect antenna structure. A reasonable poloidal distance should be left between the "corner" field lines and the antenna box, because convective cells around the antenna are larger than the box itself (see [2]). Poloidal and toroidal resolution should be sufficient to resolve small-scale antenna structures (typically FS rods). In the radial direction, it is proposed to start the mapping at the antenna mouth. No sheath will be assumed inside the antenna box. The radial extension and resolution of the map should be adapted to reproduce the evanescence of the Slow Wave. For $\varepsilon_{//}$=-24000, the radial evanescence length is approximately 6mm. It is proposed to map the RF field every millimetre over 15mm from the antenna mouth.

NUMERICAL INTEGRATION ALONG TILTED STRAIGHT LINES IN 2D

In order to prepare intensive simulations on large scale field RF maps, numerical methods for integrating RF potentials were improved towards more accuracy and reduced computing time. The new methods were benchmarked against previous ones during the preliminary study in the appendix. They are well suited for tilted straight field lines in a 2D reference plane, but could be extended to more complex 3D field line topologies if need be.

In this section we consider a scalar field $y(x_1,x_2)$ defined in a 2D space with cartesian coordinates (x_1,x_2). We seek to integrate y along a straight line tilted by an angle α with respect to the x_1 axis. y is known on a 2D rectangular grid with coordinates $x_{1a}(j)$ and $x_{2a}(k)$, (j,k) integers, dividing the 2D space into rectangles of the type ①②③④. The grid may not be regular. The integration path can be split into its successive intersections with several rectangles, which are segments of the type [A, B]. In figure 5 point A is on a

vertical grid line and point B is on an horizontal grid line, but other configurations can be imagined with A and B either on vertical or horizontal grid lines. Interpolation formulas are valid for all configurations.

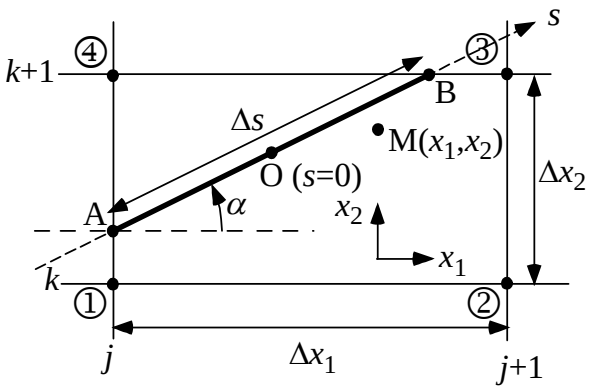

Figure 5: Geometrical notations used in integration formula

In every point M(x_1,x_2) inside rectangle ①②③④ a bilinear interpolation of y is performed from its value at grid points.
Integration along segment [A,B] thus takes the simple form.

$$\int_{-\Delta s/2}^{\Delta s/2} y(s)ds = y(0)\Delta s + \left(y_1 + y_3 - y_2 - y_4\right)\Delta s^3 \sin 2\alpha \,/\left(24\Delta x_1 \Delta x_2\right) \quad (9)$$

with

$$\Delta x_1 \equiv \left[x_{1a}(j+1) - x_{1a}(j)\right]$$
$$\Delta x_2 \equiv \left[x_{2a}(k+1) - x_{2a}(k)\right]$$

Subscripts 1,2,3,4 of y refer respectively to grid points ①,②,③,④. The above formula also applies if A and B are not located on grid lines, provided that they still belong to the same rectangle. This can be useful near end points of open field lines. If the integration path is horizontal or vertical, $\sin(2\alpha)=0$ and the integration technique is Simpson's method. The procedure of numerical integration is thus the following:

- Determine the intersection of the tilted line with horizontal grid lines, and then with vertical grid lines.

- Sort the intersection points, for example by increasing values of coordinate x_1, to split the integration path into successive segments of type [A,B].

- For each segment, determine rectangle ①②③④, middle point O(t_0,u_0)and length Δs. Perform the integral using the analytical formula (9).

- Add-up the contributions of all segments.

CONCLUSIONS

At the end of 2006 it was agreed to test the fall-back dielectric tensor on HFSS, and after assessment of the obtained RF field maps to proceed with RF sheath evaluation. Initially several antenna phasings as well as several configurations of Faraday Screen had to be compared. Since then Faraday Screen design has started. Therefore the following option was proposed:

- Start with a reference case, using "standard" toroidal phasing [0,π,0,π] and FS design currently envisaged (3rods/box, horizontal bars). This reference case will serve to assess the proposed numerical procedure, and to evaluate an order of magnitude for heat loads.

If we are confident enough on the results of the reference case, and if significant heat loads are found, then proceed with other toroidal phasings and other FS designs, specified by IT team and FS design task. To perform this work the task CEFDA05-1329 was extended till April 2007.

If field maps assessment reveals not satisfactory, it was proposed to calculate RF fields using the new antenna code TOPICA [5], which incorporates a more realistic plasma load than HFSS. This could be envisaged only within the framework of a new EFDA task.

REFERENCES

[1] M. Bécoulet, L. Colas, S. Pécoul, J. Gunn, Ph. Ghendrih, A. Bécoulet, and S. Heuraux, *Phys. Plasmas*, Vol. 9, No. 6, pp. 2619-2632, June 2002

[2] L. Colas, S. Heuraux, S. Brémond, G. Bosia, "RF Current Distribution and Topology of RF Sheath Potentials in Front of ICRF Antennas" *Nuclear Fusion* 45 (2005) 1–16

[3] D.A. D'Ippolito, J.R Myra & al. *Phys. Fluids* B5 (10), 1993, p. 3603

[4] Ph. Lamalle & al. *Nuclear Fusion* 46 (2006) p. 466

[5] V. Lancellottia, D. Milanesio, R. Maggiora, G. Vecchi and V. Kyrytsya, *Nuclear Fusion* 46 (2006) S476–S499

[6] L. Colas & al., "2-D mapping of ICRF-induced SOL perturbations in Tore Supra tokamak." Proc. 17th PSI conference, Hefei, 2006, paper P3-4, submitted to *Journal Nucl. Mat.*

[7] ITER ICRF Antenna Loading with New Limiter and Plasma (David Swain and Mark Carter), August 31, 2004

REPORTS AND PUBLICATIONS

[8] 'EFDA Task TW6-TPHI-ICFS2 - Interim Report', PHY/NTT-2006.004, June 2006
SYSSC/04-RT0143/Rev. 0 September 2004

[9] ‘Approximation of cold magnetized plasmas in the ICRF range of frequencies with a diagonal dielectric tensor’, Private communication, November 2006

TASK LEADER

Laurent COLAS

DSM/DRFC/SCCP/GSEM
CEA-Cadarache
F-13108 Saint-Paul-lez-Durance Cedex

Tel.: 33 4 42 25 65 32
Fax: 33 4 42 25 62 33

e-mail: laurent.colas@cea.fr

TW5-TPHI-ICRFDEV

Task Title: DEVELOPMENT OF HIGH PERFORMANCE TUNING COMPONENT FOR THE ITER ION CYCLOTRON ARRAY

INTRODUCTION

The Compact Vacuum Tuner (CVT) is a high power tuning device to be developed for use in the ITER Ion Cyclotron Heating launcher [1]. As such, it is designed to be compatible with ITER vessel mechanical interface, EM loads, mechanical, thermal, and nuclear specifications. On the basis of this pre-design, it was originally planned to manufacture and test a prototype component. To validate the CVT, dedicated R&D strategy to assess the most critical aspects regarding the CVT based on mock-ups was preferred to complicated test on the final object. The main uncertainties related to this high power tuning device identified are:

- The RF response of the system over the operating frequency band;
- The voltage stand-off capability of the structure;
- The operation of the RF contacts inserted in the system sliding under RF current.

The RF response with regard to frequency and geometrical variation will be validated by the mean of low power measurements on an un-cooled mock-up with a network analyzer. The same setup will also be used to assess the voltage stand-off capability of the structure, connecting the mock-up (under vacuum) to a high power RF line. A second setup, water-cooled, under vacuum and compatible with operation at high RF power for long pulse length, was also design to test the operation of the RF contact in movement.

Hereafter, the CVT inserted in the ITER IC launcher is briefly described as an introduction for the presentation of the two setups proposed to validate the system.

Description of the CVT integrated in the ITER IC antenna

The overall structure of the ITER IC launcher is described in [1], and the electrical concept of the CVT with a complete discussion on the different options can be found in [2].

From a mechanical point of view, the tuner consists in a simple coaxial structure (figure1), with an inner conductor of variable length. Between the two conductors a contact support actuated by 2 rods can be moved independently from the inner conductor variation. The two movements are guided by bearings and ball screws located behind the contact support, and isolated from the torus vacuum by metallic diaphragm bellows. The variable position of the electric short circuit inside the tuner coaxial structure, combined with the movement of the inner conductor will allow an appropriate matching range.

The CVT is an “LC type” matching system featuring a capacitive or inductive behaviour depending of the relative position of the inner conductor and short-circuit. By its conception, the CVT is robust structure that can be manufactured without many difficulties, the only remaining uncertainties on the CVT are its RF behaviour. Two dedicated test rigs were designed and are under completion to assess this specific aspect.

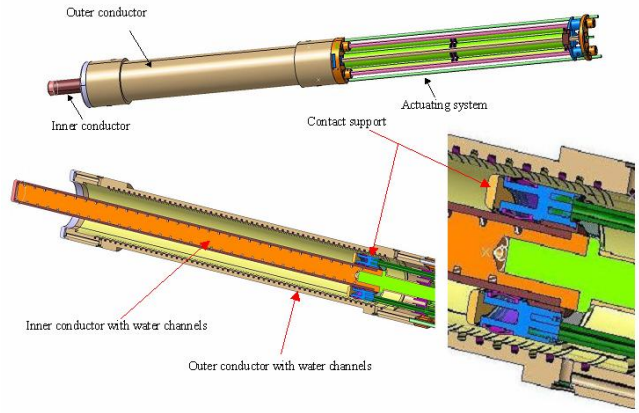

Figure 1: View of the CVT structure integrated in the ITER IC launcher

Voltage stand-off and low-power measurement setup description

On the basis of the clearance of the structure inserted in the ITER IC antenna, a mock-up with the same outer structure (geometrical envelop) of the CVT was designed (figure 2 and 3). The mock-up proposed will allow the test of the following electrical configurations (depending of the relative position of the inner conductor and short-circuit): purely inductive (L), purely capacitive (C), and the LC configuration a combination of the two.

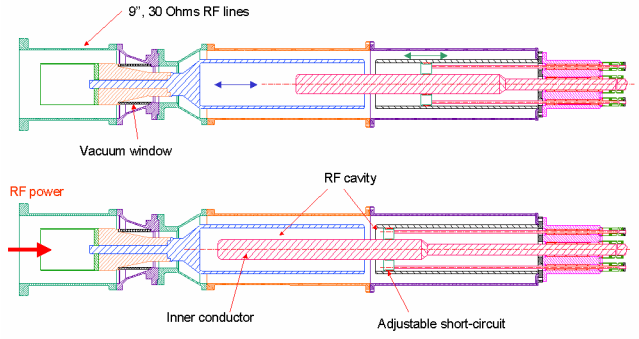

Figure 2: Cut-view of the CVT mock-up

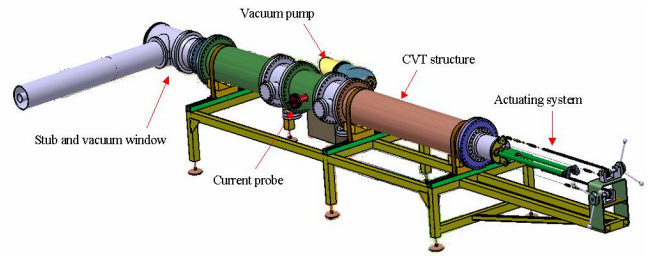

Figure 3: Over-view of the CVT test-rig

A first series of low power measurements will be conducted over the operating frequency band (40-55MHz) prior to high power tests. For the voltage stand-off qualification, RF power shots lasting a maximum of 10s will be sufficient. An un-cooled structure can therefore be used to work on this specific problematic. For the tests, the existing Tore Supra test bench will be used, with the experimental setup short-circuiting the 30Ω coaxial lines connected to one of the TS RF generators (figure 4). On this test bed, RF pulse of 40kW with peak voltage of 40kV, and peak current of 1.4 kA RMS can be routinely achieved fur duration of 60s. The experimental setup will be instrumented with bi-directional couplers located prior to the vacuum window, voltage and current probes located under vacuum, and vacuum probes will monitored the vacuum level during operation.

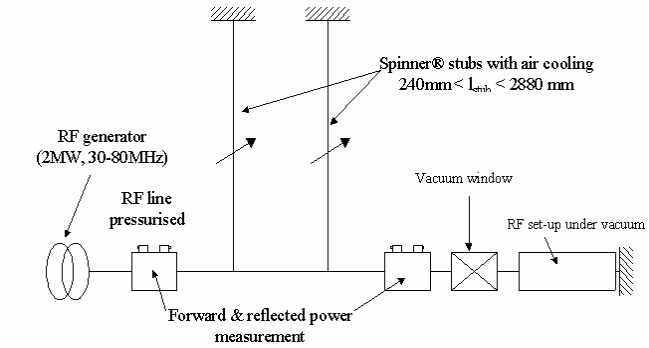

Figure 4: Sketch of the high power test-bed

Test of the sliding RF contact in baked environment under vacuum setup description

The flexible Finger Contacts (FC) integrated in the design of the antenna are MC®-Multilam™ LA-CUT/0.25/0. These FC have been chosen for of their electrical, thermo-mechanical and geometrical properties, i.e: low contact resistance, high current-carrying capacity, large temperature range of utilization, large radial tolerance and angular misalignment absorption. These properties result of the original design of the FCs consisting of 1mm thick louvers made of silver-plated copper mounted on a 0.3 mm stainless steel carrier strip. In the LA-CUT contact the contact pressure is ensured by the slightly bended SS strip, this feature allowed more severe working conditions in term of temperature than the standard copper beryllium thin strip of contact. These contacts have been successfully tested at CEA-Cadarache under vacuum and high temperature, within different assembly geometry [3], [4].

In order to check the mechanical integration of the contact in the CVT configuration small, mock-ups of the contact support has been fabricated (figure 5). The remaining uncertainty is their operation sliding with RF power applied.

Figure 5: Assembly mock-up of the MC contact

In the setup sketch in figure 6, the contact will be tested sliding under vacuum at a maximum of current (short-circuit of the line), within a mechanical configuration similar to the one integrated in the IC launcher. The two FC strips are inserted in a Ø54mm groove, one located in the short-circuit, the other few centimeters away inside the inner conductor. A cylindrical axis, connected to a step-motor by the mean of ball screw, slide in between the two FC strips. The contacts are cooled on both sides (shaft/groove) in a similar configuration than the one proposed on the antenna. The TS test bench will be used for the test, the pulse length for the tests will be limited to a duration of 60s, with a heavy cycling.

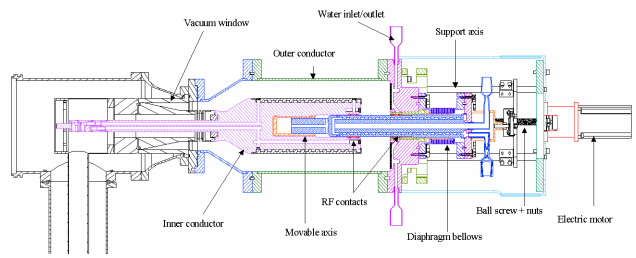

Figure 6: Sketch of the high power test-bed

CONCLUSIONS

Once all the tests completed, the manufacturing of a complete prototype component can be planned, to assess the mechanical interface of the CVT with the actuating/driving system. The results and knowledge harvested during this R&D program, in complement to the on-going studies carried out the IC launcher, will give all the required technical elements to launch the manufacturing of a series CW CVT applicable for use in ITER.

REFERENCES

[1] EFDA Task 05/1271 - First Interim Report, K. Vulliez, G. Bosia, G. Agarici, A. Argouarch, P. Testoni, D. Milanesio, R. Maggiora.

[2] A coaxial vacuum tuner for fusion application, G. Bosia ref IRGB 06/01.

[3] Report on EFDA 02/670 contract /deliverable E4A: JET-EP ICRH antenna finger contact tests, K. Vulliez, P. Mollard, S. Brémond.

REPORTS AND PUBLICATIONS

[4] Test des contact Multilam® sous-vide pour la connectique de ligne HF au standard 9‘’, K. Vulliez, P. Mollard, internal CEA report CH-NTT-2006-029.

TASK LEADER

Karl VULLIEZ

DSM/DRFC/SCCP/GCHF
CEA-Cadarache
F-13108 Saint-Paul-Lez-Durance Cedex

Tel. : 33 4 42 25 73 19
Fax : 33 4 42 25 62 33

e-mail : karl.vulliez@cea.fr

CEFDA03-1111Bolo

Task Title: TW3-TPDS-DIASUP1: SUPPORT TO THE ITER DIAGNOSTIC SYSTEM: BOLOMETER ARRAY

INTRODUCTION

Europe has a long standing leading role in bolometer development towards the reference design for ITER (e.g. [1], [2]). This has been continued by the EFDA with contracts on further development of this diagnostic [3], [4], [5] including the present one. This contract was aimed at the investigation of the survivability of the reference bolometers considering two substrate options - the standard 20 µm Mica foil and a new 1.5 µm SiN carrier [5] - in abnormal conditions as during disruptions or high EC-power (at 170 GHz) incidence and consequences for the design in particular for the viewing apertures. Some reflections on connectors and cabling and on a plan for the full development towards ITER were also demanded. The draft final report on this task has been submitted to EFDA November 2006 [8].

2006 ACTIVITIES

The investigation of the disruption survivability started with an analysis of the disruption phenomenology. A disruption may begin with a precursor phase (100ms) during which mitigating measures such as heavy gas puffing can be employed. If this has no effect the disruption continues with a rapid (0.5-3 ms) thermal quench during which the electron temperature drops to 3-10 eV and a major fraction of the thermal energy (1 GJ) hits the divertor. Thereafter the current quench sets in with a current quench rate of up to 450 MA/s during 50 – 200 ms which may lead to runaway electron currents (up to 16 MA). A loss of vertical stability (VDE = vertical displacement event) may also occur at one stage or other of the disruption. It will induce eddy currents in the vessel that may lead to strong forces on the vessel (150 MN). For our investigation we chose the most severe of the conditions in each of the phases.

The investigation of the currents induced in the absorber of the bolometer during the current quench phase due to eddy currents in the absorber itself and in the camera box and halo currents in the wall lead to an estimation of a maximum current of the order of 100mA. The forces and the stress and the strain on the foil were calculated on the basis of the maximum current in the foil and were found to be more than 3 orders of magnitude lower than the limit for Mica which is of the order 100 MPa. The maximum induced current value in the CuCrZr base plate had earlier been estimated to 3620 A [3]. Even with this current the strain on the baseplate rests (with 2 MPa) more than one order of magnitude below its limit.

We considered the case of a disruption mitigation technique using massive gas injection of about 1 kg of He. For such a scenario we estimate a pressure rise in 1 ms to 200 mbar. The Mica foil can only withstand 60 mbar. We propose to introduce holes in the camera box and the base plate that reduce the strain to 4 MPa for the mica foil and to 64 MPa on the thinner SiN foil, which is largely acceptable for the mica foil, but should be looked into more detail for the SiN carrier foil since it is more marginal there (safety factor 1.5).

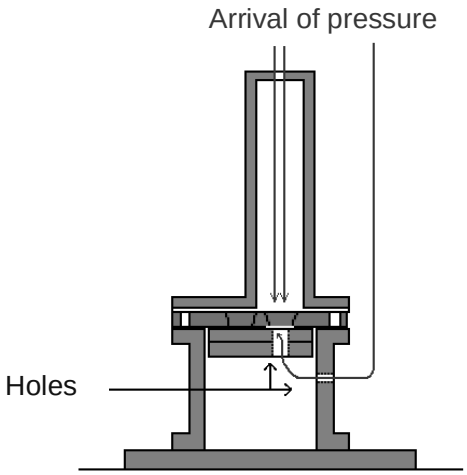

Figure 1: Equalisation of pressure

For the acceleration of the part of the vacuum vessel on which the bolometers are mounted we estimated a maximum of 15 g (including a security factor of 2-3) which gave us a securite margin of 2 orders of magitude for the Mica foil and one order of magnitude for the SiN foil.
Having seen that the current quench phase will be survivable by a large margin we looked for the effects during the thermal quench phase and found that the temperature rise due to the intense radiation (400MJ assumed) will be below 100°C for the absorber foil. Similar values had been found previously for the temperature rise of the front-end of the camera-box [3]. These values are acceptable.

With regards to the interference of EC waves we considered as the worst case scenario that EC waves may land (attenuated to 5%) on a bolometer. This would be a potential power density of 6 MW/m², which would lead to a power deposition in the absorber of 50mW, which is at almost 2 orders of magnitude higher than typical radiation signals, normally measured by the bolometers. The proposed protection is to make many small openings instead of 1 large one and to form the openings such that become underdimensioned and therefore attenuating waveguides for the EC waves of a wavelength of 1.8 mm. A system of 12 such waveguides (figure 2) of 3 mm length and 0.5 mm width in poloidal and toroidal directions has an attenuation of power of 58 dB which would be largely sufficient.

The principle of such a collimator structure is shown in figure 3. The upper apertures have a microstructure as indicated in figure 2. The lower apertures are open and serve to avoid cross talk between the channels.

The comparison of the light transmission achievable with such multihole apertures in relation to the values achievable with single hole pinhole constructions as assumed in the previous tomographic perfomance analysis [4], has led us to estimate the losses of light to be 20 % - 50 % depending on the respective camera position.

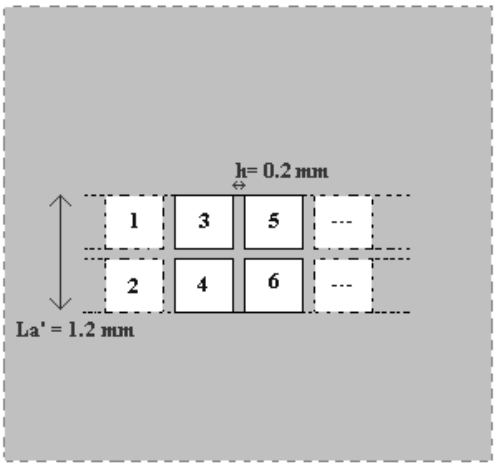

Figure 2: System of multiple slit apertures

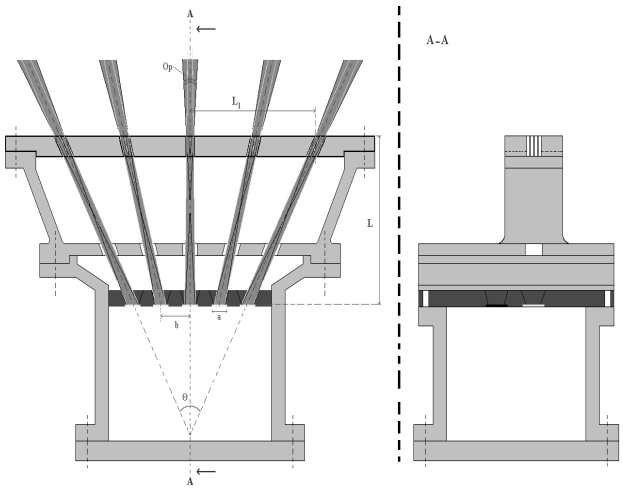

Figure 3: Architecture of a camera with a multiple slit aperture system

From JET experience some recommendations for cabling and connectors were given:

1) Wherever possible solid metal-metal joints such as soldered, welded or bonded connections should be used. Spring connections should be avoided wherever possible.

2) Another principle that is important in this respect is the use of the highest possible voltage on the detector foils in order to have the best possible signal/noise ratio.

3) As far as the choice of cables is concerned it is worth the effort to find out how close one can bring the organic isolated cable type which is used in ASDEX Upgrade and in JET for the vertical X-point camera KB5 to the bolometers in order to keep the length of the more noisy but more radiation resistant ceramic cable (as used for the in-vessel JET bolometers) as short as possible.

CONCLUSIONS

The research activities towards ITER should in the first instance continue with the irradiation programs of alternative substrates AlN and SiN with metallic parts in Pt. In the more distant future the ferrolectric bolometers [6] may play a role, but a considerable effort is still needed to bring them to the usability of the conventional bolometers. In the course of this report we have identified the thickness of the SiN substrate as relatively thin in comparison to the thickness required to withstand disruption mitigation. This should be investigated in more detail. The cabling question needs more attention.
More advanced than the ferro-electric bolometers are the 2D-IR bolometer cameras [7]. They look like a more realistic and faster track to working alternative bolometers. The main questions are the attainable sensitivity and calibration issues.

REFERENCES

[1] 'A low noise highly integrated bolometer array for absolute measurement of VUV and soft x radiation' K.F. Mast et al., Rev. Sci. Instrum. 62 (1991) 744

[2] 'Bolometer for ITER', R. Reichle, J.C. Fuchs, R.M. Giannella, N.A.C. Gottardi, H.J. Jaeckel, K.F. Mast, P.R. Thomas, in: Diagnostics for Experimental Thermonuclear Fusion Reactors, eds. P.E. Stott, G. Gorini and E. Sindoni ,Plenum Press, New York, (1996) 559

[3] 'Thermal analysis of the ITER reference bolometer', J.C. Vallet, C. Portafaix, EFDA report for task 02-1003 (2004)

[4] 'Optimisation of the Detector Arrangement of the ITER-FEAT bolometric Diagnostic' S. Kàlvin, EFDA report 11/2002

[5] 'Prototype of a radiation hard resistive bolometer for ITER' L. Giannone, D. Queen, F. Hellman, J.C. Fuchs; Plasma Phys. Contr. Fusion 47 (2005) 2123

[6] 'Ferroelectric Bolometer', M. Di Maio, R. Reichle, UK Patent application, provisional no: 9623139.4, Nov. 1996

[7] 'Radiated power profile observed by tangentially viewing IR imaging bolometer in JT-60U tokamak' S. Konoshima, B.J. Peterson et al., Contr. 32nd EPS on Plasma Phys., Tarragona 27 June - 1 July, ECA 29C P-4.092 (2005)

REPORTS AND PUBLICATIONS

[8] Detailed Design analysis of bolometer cameras on the basis of the reference resistive bolometer sensor', R. Reichle, S. Hourcade, EFDA report for task 03-1111 (2006) and CEA note DIAG/NTT-2006.021

TASK LEADER

Roger REICHLE

DSM/DRFC/SIPP/GID
CEA-Cadarache
F-13108 Saint-Paul-lez-Durance Cedex

Tel. : 33 4 42 25 63 76
Fax : 33 4 42 25 49 90

e-mail : roger.reichle@cea.fr

CEFDA03-1111WAVS

Task Title: TW3-TPDS-DIASUP1: SUPPORT TO ITER DIAGNOSTIC SYSTEM: ITER WIDE-ANGLE VIEWING THERMOGRAPHIC AND VISIBLE SYSTEM: OPTICAL DESIGN

INTRODUCTION

The task consists in performing an optical design for the ITER wide-angle equatorial viewing system (Procurement Package: PP5.5.11 – G01 Equatorial Visible-IR TV). This system is proposed to ensure visible and IR real time survey for machine safety and operation. The ITER equatorial viewing system is presently composed of 3 different views (tangential left, tangential right and divertor views) into 4 different port plugs (Port Plug EQ#01, 03, 09 and 12). The field of view for the EQ#01 RIGHT tangential view is presented in the figure 1. Blue dash lines indicate the high field side pellet injection.

Figure 1:

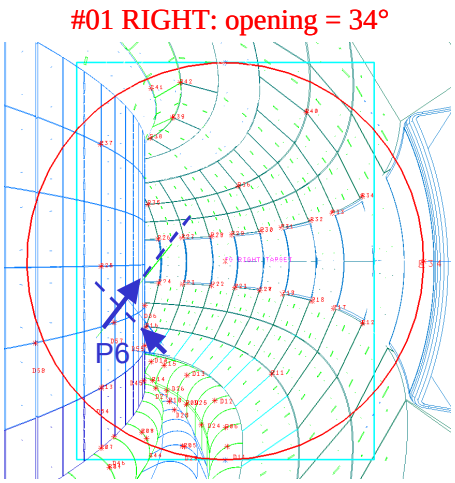

2006 ACTIVITIES

The activity done in 2006 concerning this task was essentially dedicated to the writing of the final report for EFDA. This has been done by CEA in close contact with C. Walker from the ITER diagnostic team. In this technical fusion report we'll give a description of the optical and mechanical design with the associated performance of the system. At the end of this document, we'll propose a list of remaining things to be addressed to develop the diagnostic.

The technical specifications of the system are the following:

- The system has to provide good measurements of the surface temperature in the range of [200-2500°C] with a large field of view, with the required spatial (for hot spot) and time resolution (10ms).

- The second function of the system is also for machine safety and operation, but in the visible range (UFOs, initial wall-damage assessment).

- This diagnostic can alternatively be used to study runaway electrons, visible spectroscopy or/and track pellet.

- This diagnostic can also be used for other physic purposes (heat loads and particle balance, dust and layer localisation…). In his present requested form, this diagnostic doesn't resolve transient events (ELM and disruption).

DESCRIPTION OF THE OPTICAL DESIGN

Several optical solutions have been investigated. The final solution has been selected by taking into account: 1) the available volume into the port plugs, 2) the expected performance of the system and 3) the complexity and feasibility of the solution. According to us, the best solution today is a single optical line with a double Cassegrain embedded one into the other one (solution with a hole in the optical throughput): one large Cassegrain for the IR light (diameter: Φ_{IR} = 10 cm), into which is inserted a smaller Cassegrain for the visible light (diameter: $\Phi_{visible}$ = 2 cm). The main advantage of this solution is the reduced required volume. The anti-reflection coating is not a problem in that case and could be adapted to the light (IR in the outer periphery and VIS in the inner periphery of the optical beam). On the other hand, mechanic and tolerencing of the optical system will be more challenging.

The full optical design for the 3 different views into port plug EQ#01 is presented in the figure 2. The proposed generic optical line is compatible with port plug #01, #03, #09 and #12. Each line is essentially composed of: the head mirror assembly facing the plasma, one double Cassegrain telescope, one adaptative relay to put the image up and one sub-marine like standard relay to accommodate the machine displacement relatively to the bio-shield.

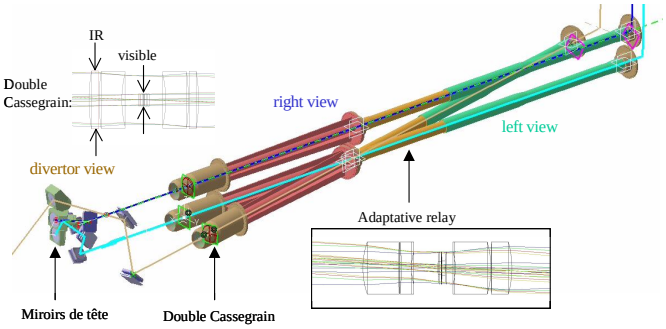

Figure 2: Full optical design

OPTICAL PERFORMANCES

The performance analysis shows that, with a numerical aperture of 3.3, the maximum of resolution of the system is:
- 1800 points at 3µm and 1080 points at 5µm for the IR part
- 3375 points at 400nm and 1928 points at 700nm for the visible

These resolutions satisfy the requested specification. A detailed study of the spatial resolution on the ITER first wall shows that about 80% of the inner wall is visible with a reasonable spatial resolution (≤ 9mm). The main chamber is particularly well covered but the divertor region is much less covered because of the line of sight that is not optimized for this part of the machine. The equatorial wide angle viewing system cannot replace the divertor thermography, especially in the outer leg (one of the crucial part of the machine). The spatial resolution of the full WAVS system over the full first wall of the machine is presented in the figure 3 in the (φ,θ) plan.

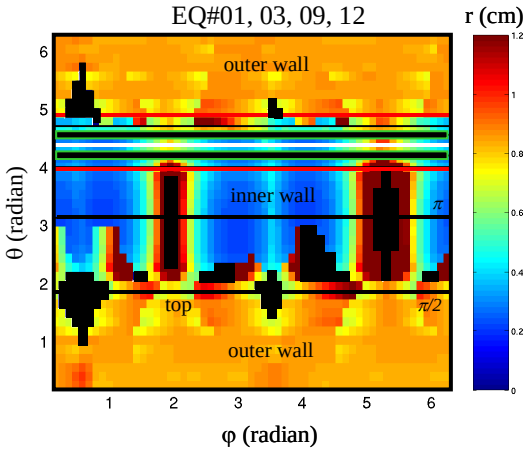

Figure 3: Spatial resolution of the full WAVS system

The spatial resolution lies between [3-5] mm on the inner wall and [7-9] mm on the outer wall. About 80% of the first wall is viewed.

MECHANICAL DESIGN aND INTEGRATION

A simplified mechanical design is proposed to reserve the needed volume for the VIS/IR wide angle viewing system. This preliminary mechanical design is shown in figure 4. It is based on approximative value for each optical component, no thermal analysis have been performed and take into account in the present form of the mechanical design. The needed diameter into the port plug is ∅=240mm at the double Cassegrain location, note that this is into the port plug that the available space is the most demanding. The needed diameter in the rest of the system is smaller and should not be a problem (~140mm at max).

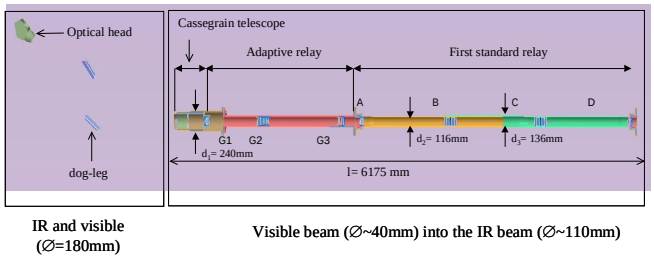

Figure 4: Preliminary mechanical design

Because of the high neutron heat flux present in the front of the port-plug, the most crucial part of the mechanical design is the head mirror assembly - made of one aspheric and one flat mirror. In its present form, the mechanical design is made of 3 separate and identical head mirror assembly. An integrated box design has to be done with efficient water cooling (note that this part should be accessible for maintenance: mirror cleaning or mirror changes). This is illustrated in figure 5. Thermal analysis have been started to dimension and design the box with an adapted active cooling system.

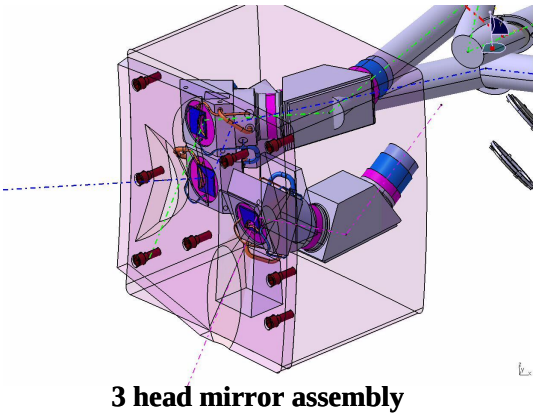

Figure 5

The integration of the 3 optical lines including the simplified mechanical design into the port plug EQ#03 is presented in the figure 6 with the neighbourhood diagnostics. Because of the charge exchange and H_α diagnostics, the available volume for IR-VIS wide angle viewing system is very limited. The available volume is also very limited in port plug EQ#01.

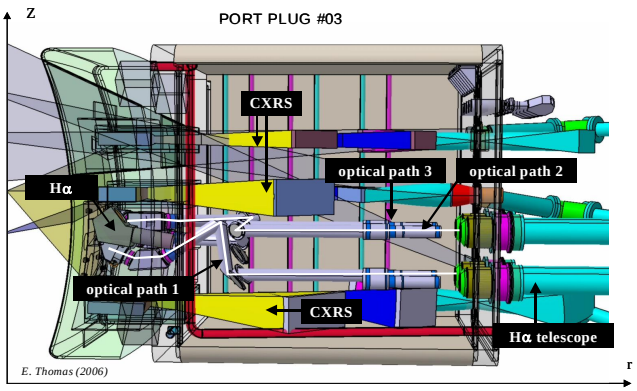

Figure 6

COORDINATION AND OTHER TASKS

As the leader Association, Euratom-CEA was also responsible for coordinating the other tasks related to the equatorial wide angle viewing system:

Assess the efficiency of the visible imaging
This task is contracted by ENEA. For the main chamber the system seems:
- Adequate for D_α measurements
- Rather marginal for detecting carbon and beryllium influxes
- Not adequate for tungsten

For the divertor the IR-VIS system is:
- Adequate for D_α and C influx (at least for the plain solution)
- Marginal/adequate for detecting beryllium and tungsten influxes

Assess if the system can be used to study runaway electrons:
This task has been contracted by FOM institute. It shows that the present version of the optical design is well adapted to measure synchrotron radiation in the band: 4-5 μm.

Assess if the system can be used to study pellet injection:
This task has been contracted by CEA. It shows that the present version of the system is very well adapted to track pellets.

Assess if the equatorial wide angle viewing system can supplement or replace the divertor thermography:
This task was supported by CEA. It has been shown that the equatorial system is not adapted to survey the vertical tiles on the outer side (low field side) of the divertor. A region where the deposited heat fluxes can be very important (outer strike point).

REMAINING TOPICS TO BE ADDRESSED:

For the optical/mechanical design:
1. Test wide band Visible and Infrared antireflection coating for lenses. Simplified architecture. Reduction of Optical and Mechanical tolerances. Large increase of the Visible performances (but not the IR).
2. If point 1) failed, test the Holographic selective diffuser solution. This is an interesting alternative.
3. Optical generic line choice and optimisation.
4. Test the auto-adaptative shifting relay. Solution more reliable than active method.
5. A mechanical design should be done when points 1) to 3) will be achieved.
6. Shutter development generic for all optical diagnostic (ENEA task).
7. Data acquisition.
8. Data storage.
9. Database and data management.
10. Access to the database.
11. Design a test-bed.
12. Build the prototype.
13. Test the prototype in an adapted environment / acceptance criterion.
14. Feed-back on the optical/mechanical design.
15. Make an up-date of the optical/mechanical design.
16. Ready for construction... and, some months later, ready to be installed in ITER.

For the *IR* and *visible* measurement: "metrology"
1. The transmission of the system is expected to vary with time. We need to measure the global transmission for calibration of the system. This could be done:
   In situ: calibrated black body/spectral source with the articulated inspection arm (for VIS and IR)
   During operation: heated tile with TC, heated shutter with TC (for IR).
2. Assess to the head mirror assembly: Cleaning of the mirror.
3. Evaluation of the temperature incertitude (for IR).
4. Passive/Active method to measure emissivity (metals, co-deposited layer characteristics) and so improve temperature measurements (for IR).
5. Study the 2 wavelengths system to improve temperature measurements (for IR).
6. Assess the problem of reflection in metallic environment (for VIS and IR).
7. Develop tools to simulate VIS and IR pictures (ray tracing) with simplified models of the Vacuum Vessel and inner components could also be very helpful for optimisation of the optical design.

REPORTS AND PUBLICATIONS

[1] 'ITER wide-angle viewing thermographic and visible system: optical design', EFDA final report, submitted December 2006

[2] "ITER wide-angle viewing thermographic and visible system"; D.Guilhem, Y.Corre and al.; CEA internal reports DIAG/NTT-2007.002 and DIAG/NTT-2007.003

[3] "Can reflections strongly modify the measured surface temperature of plasma facing components in experimental fusion reactors like Tore-Supra, JET and ITER ?" 8th Int. Conference on Quantitative Infrared Thermography (2006); D.Guilhem, R.Reichle, H.Roche

[4] "Reflections and surface temperature measurements in experimental fusion reactors Tore-Supra, JET and ITER"; D. Guilhem, R. Reichle, H. Roche QIRT Journal. Volume 3 N° 2/2006, pages 155 to 168

TASK LEADERS

Dominique GUILHEM

DSM/DRFC/SCCP
CEA-Cadarache
F-13108 Saint-Paul-lez-Durance Cedex

Tel. : 33 4 42 25 62 32
Fax : 33 4 42 25 62 33

e-mail : dominique.guilhem@cea.fr

Yann CORRE

DSM/DRFC/SIPP
CEA-Cadarache
F-13108 Saint-Paul-lez-Durance Cedex

Tel. : 33 4 42 25 49 81
Fax : 33 4 42 25 49 90

e-mail : yann.corre@cea.fr

CEFDA05-1343MS
TW5-TPDS-DIADEV

Task Title: TW5-TPDS-DIASUP1: DIAGNOSTIC DESIGN FOR ITER: MAGNETIC SENSORS

INTRODUCTION

The EU will supply the magnetic diagnostic for ITER. In 2005, a review and design analysis of the ITER magnetics diagnostics has been carried out [1–6]. While the magnetic diagnostic includes a wide diversity of sensors in interaction with the ITER vacuum vessel and located in various places, the task involves 4 partners: EPFL-CRPP which ensures the task coordination, ENEA-RFX, CEA and CIEMAT. It is also conducted in very close interaction with the ITER international team.
The objective of the 2006 activity deals with the analysis of the magnetic diagnostic general design focusing on ex-vessel tangential and normal coils (A.01), external continuous Rogowski loops (A.04) and fibre optic current sensor which were recently considered for plasma current measurement. The overall activity aimed at:

- Designing underdeveloped sensors considering environmental conditions and interface with tokamak components.
- Developing ElectroMagnetic model for vacuum vessel movement and current.
- Initiate the performance analysis on the sensor
- Complete the existing technical description documents to a more detailed level
- Update and refine the work plan for full implementation of the magnetics diagnostic on ITER
- Assess the existing documentation and assist the ITER IT in the updating of the documentation.

2006 ACTIVITIES

EX-VESSEL TANGENTIAL AND NORMAL COILS

The ex-vessel coils radial and tangential coils set-up is a supplementary set used to measure the plasma current, position and shape. It requires higher signal level than in-vessel coils set-up in order to improve the measurement errors. The requirement is to build coils with an effective area of $2m^2$. Originally, the available winding pack was $7x55x250mm^3$. It was shown [4] that making a $2m^2$ area tangential coil in such small winding pack is very hard (easier for radial coils). In fact the main constraint concerns the radial dimension (8 mm) that cannot be enlarged to keep sufficient clearance between the VV outer shell and the thermal shield. More space is available along the toroidal direction; therefore the winding pack has been enlarged to $9x159x250\ mm^3$ in areas where the radius of curvature of the vacuum vessel is big and $9x155x122\ mm^3$ in areas where the radius of curvature of the vacuum vessel is smaller (figure 1). Coils have been fully redesigned. Their ellipticity has been substantially increased compared to the previous design.

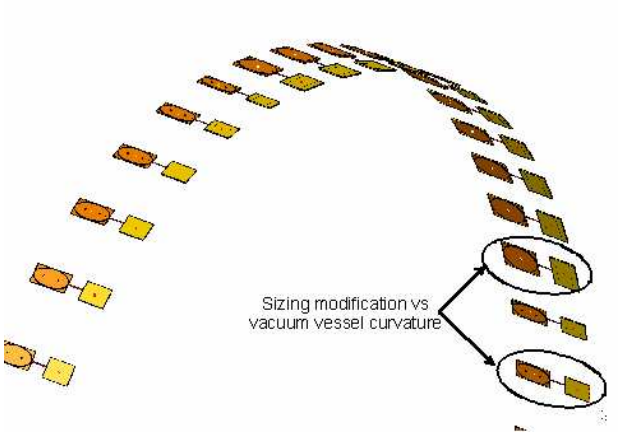

Figure 1: Illustration of coils integration on vacuum vessel

This was possible because we proposed to wind the coil as a transformer without trying to arrange each turn in order to fill entirely a layer. We specified the number of turn per layer which is smaller than the maximum number of turn available. For example, while the coil can accommodate 700 turns per layer we specified only 650 turn per layer. With such geometry it is possible to use 0.35mm OD enamelled cable instead of 0.25mm (previous design) ensuring a more robust coil. Using such winding process, freedom is left to the cable with respect to the coil former requiring to “pot” the coil into its casing with a ceramic filler. This winding technique prevents getting a constant coil effective area over the 60 sensors. This is not a real problem because each coil will be calibrated and their effective area will be determined. The effective area distribution will be simply larger. Prototype of ex-vessel tangential has been made (figure 2) by CEA and contact with manufacturer has been taken to produce such coil in larger quantities.

Figure 2: Photo of ex-vessel tangential coil prototype (located in large curvature vacuum vessel area)

The main electrical parameters of the coils have been calculated:

	Tangential coil (big)	Tangential coil (small)	Radial coil (big)	Radial coil (small)
Cable OD	0.35 mm		0.55 mm	
Cable type	Enamelled wire			
OD (mm^3)	9x159x250	9x159x122	9x219x219	9x119x219
#layers	4	4	6	6
Turn/layer	650	320	10	10
Effective area (m^2)	2.66	1.31	2.14	1.14
Length of cable (m)	860	425	41	32
Resistance (Ω)	210	102	3.5	2.73
Inductance (mH)	30.16	14.45	0.86	0.59

The accuracy of magnetics reconstruction is assessed using the equilibrium reconstruction code EFIT_ITM [5]. As a starting point we use a full equilibrium reconstruction calculated by DINA-CH (we used the equilibrium number 11 corresponding to plasma equilibrium on the current flat top (I_p=15MA) during the burning phase (β_p=0.43)). This gives, in particular, the flux function everywhere in a poloidal plane and the magnetic at the sensors location defined in DINA-CH. A set of relevant parameters have been defined and used to quantify the error introduced by a sensor failure. Pertinent parameters are:

- The magnetic axis positions R_{mag}, Z_{mag},
- The X-point position R_{Xpts}, Z_{Xpts}.
- The safety factor at the plasma centre q_0 and at the plasma edge q_a.
- Gaps between the limiter and the plasma boundary. As a staring point one chose the gaps defined in [6] (figure 3).

The calculated errors must be compared to the specification (1cm maximum admissible error) given in [7].

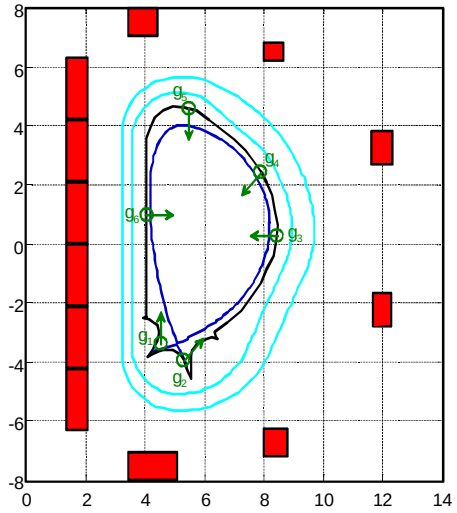

Figure 3: Gap position

Nowadays, EFIT-ITM performs simulation taking into account in-vessel sensors (12 divertor coils + 36 in-vessel coils), one complete flux loop, 23 saddle loops, 60 ex-vessel tangential coils and 60 ex-vessel radial coils. Simulations have been performed using the entire set of sensors or only the ex-vessel set.

For both cases, reference equilibrium is calculated. From it, the equilibrium accuracy has been assessed considering various defaults on one ex-vessel sensor (in-vessel sensors effects are estimated in [8]) and calculating discrepancies between the relevant parameters:

- One ex-vessel sensor is not considered in EFIT for the equilibrium reconstruction. Errors on the selected relevant parameters are small (error on gaps < 0.1mm).
- An error of 5% on the measured magnetic field is added sequentially to each ex-vessel sensor. The error on gaps is bigger and reaches 5mm.
- An offset of 10mT is added sequentially to each ex-vessel sensor. The error on gaps is lower than 1mm (figure 4).

The results obtained confirm that combining in-vessel and ex-vessel sets of coils allows more accurate reconstruction. They allow locating sensors that impact on the accuracy.

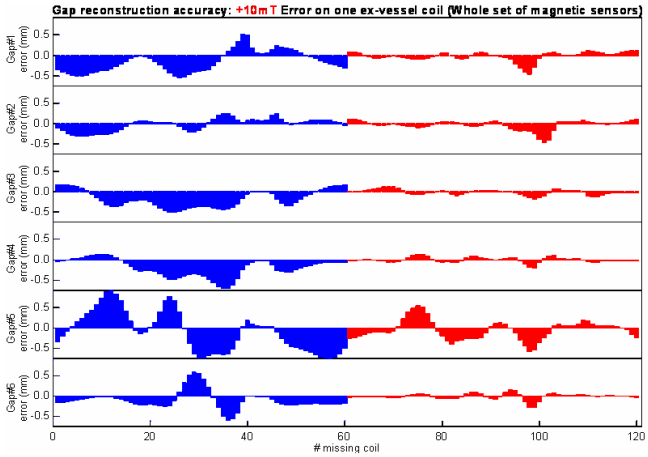

Figure 4: Example of gap errors introduced by 10mT offset on one ex-vessel coil (ex-vessel tangential coils are labelled1 to 60, ex-vessel radial coils are labelled 61 to 120)

EX-VESSEL CONTINUOUS ROGOWSKI

The external continuous Rogowski is a separate backup facility measuring the plasma current. It provides a potentially valuable backup in case of drift of the in/ex-vessel systems for long pulse operation. The set-up is located in a 14.5mm diameter groove cut in the Toroidal Field Coil (TFC) casing. The path of the Rogowski in the groove has been precisely defined (figure 5).

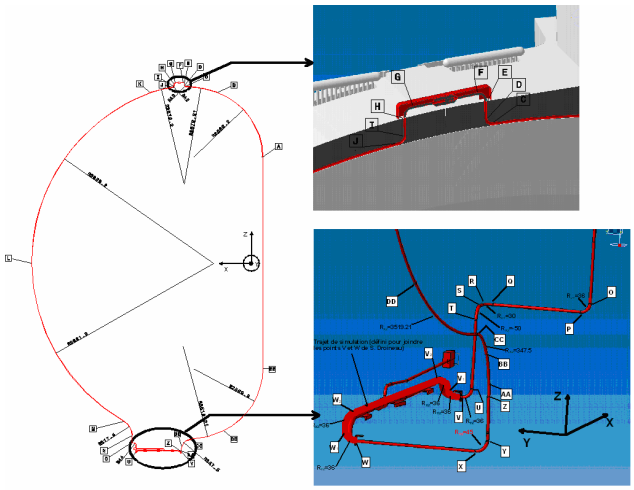

Figure 5: Rogowski path in TFC casing

The Rogowski cable is a 1mm Outer Diameter (OD) enamelled cable and fibre optic current sensors (cf. next section) must be installed in the core of the Rogowski. Therefore, the design of the Rogowski has to evolve. We analyzed an integrated solution based on composite cable (figure 6). The cable integrates a 1.0mm OD copper conductor (Rogowski cable return) and 5 to 6 optic fibres. The outer diameter of the heterogeneous cable is 9mm. A 1.0mm OD copper cable is wound like a spiral (pitch=1.05mm) on the composite cable and covered by a protective insulating sheath

The main issue of such Rogowski is the connector at the top of the TFC casing that accommodates optics fibres and copper conductor. While electric connection is easily done, the optical connection seems much more complicated. This point needs R&D or a prototype. Finally, the minimum radius of curvature of such cable is still to be assessed.

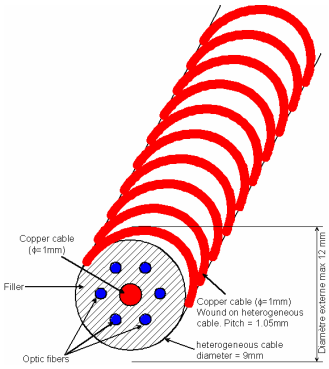

Figure 6: Example of Rogowski based on composite cable

In order to satisfy the measurements requirements given in [7], winding constraints must be defined. The Rogowski has been modelled in 3D using matlab®. The 3D magnetic field is calculated (figure 7) considering current loops accounting for tokamak systems (poloidal field (PF) coils, central solenoid (CS) and plasma current). PF coils and CS are modelled using coil positions and number of turns in each coil [9]. The plasma is modelled as a single current loop holding the total plasma current and located at the plasma magnetic axis. The time evolution of the current flowing in PF coils, CS coils and in the plasma is taken from the ITER standard scenario [9].

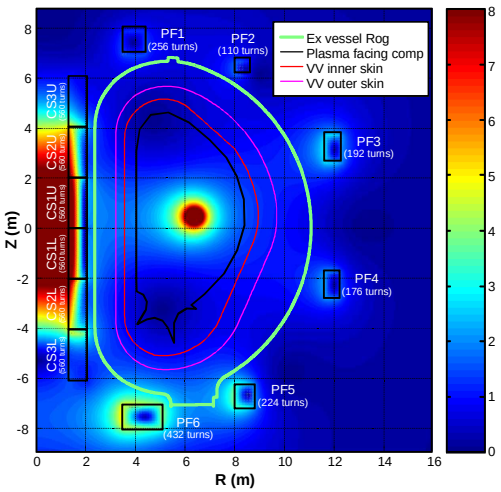

Figure 7: Magnetic field created by PF coils, CS coils and plasma current (ITER reference scenario t=300s, Ip=15MA)

Various types of winding errors have been investigated:

- Non stationary pitch between turns of cable (varying pitch along the Rogowski). The pitch mean value is set to 1.1mm. The perturbation is defined in such a way that the perturbation mean value is equal to the pitch without perturbation (1.1mm). Thus increasing the distance between turns in some places implicates that the distance is reduced in other places. The minimum distance is the cable diameter (1.0mm).
- Lack of turn along the Rogowski. Such default could simulate upper and lower joint of the Rogowski. The pitch angle is constant to 1.1mm and at a defined place 10 turns are removed. This corresponds to an empty space of 11mm (typical value we can guess for a joint). In order to identify the most sensitive parts, the location of lack of turn is moved along the Rogowski. The maximum absolute error is defined for plasma current lower than 1.0MA and the maximum relative error is calculated for current above 1.0MA. Results are shown in Figure 8 where the points account for the perturbation position along the Rogowski and the colour indicate the error amplitude.

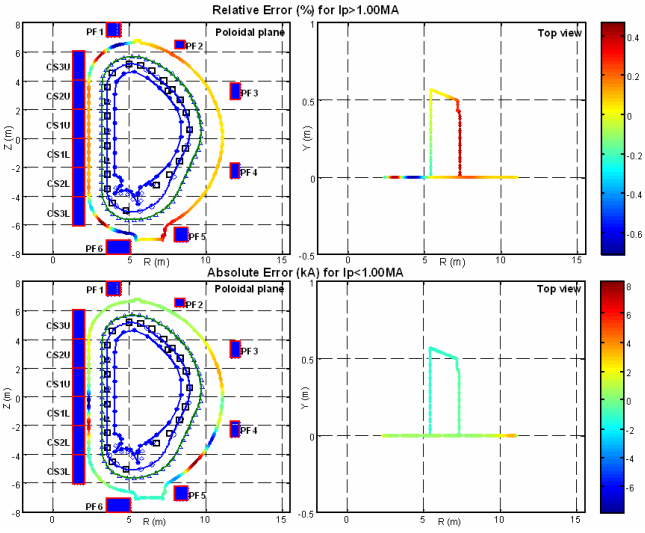

Figure 8: Absolute and relative errors due to a lack of 10 turns

Below 1.0MA, the maximum absolute error is about 8kA, satisfying ITER specifications [9]. The error is especially big when the perturbation is close to the central solenoid and PF4 and PF5 coils. The part of the Rogowski along the toroidal direction is not a source of error.

Above 1.0MA, the maximum relative error is lower than 1% satisfying ITER specifications [9]. The error is especially big near PF and CS coils. The error is also big when the lack of turn is located in the part of the Rogowski located along the toroidal direction

FIBRE OPTIC CURRENT SENSORS

Recently Fibers Optic Current Sensors (FOCS) have been considered to be installed for measuring plasma current and vacuum vessel current. The present position of the fibre could be in the core of the Rogowski (at low temperature, 4K) and along ex-vessel tangential and normal coils (at high temperature < 240°C).

The measurement is based on the Faraday Effect. In presence of a magnetic field, a linearly polarized light experiences a non reciprocal rotation of an angle proportional to the magnetic field:

$$\theta = V \oint \mathbf{H} \cdot \mathbf{dl}$$

Where V is the Verdet constant (magneto-optic constant) for the fibre material. The Verdet constant V is the specific rotation of a material and is defined as the angle over the magnetic field times the length (°/T m).

Considering a closed loop of fibre, according to the gauss theorem, this angle is simply proportional to the electrical current flowing through the sensing coil. FOCSs measure the exact integral of the magnetic field along the closed loop created by the fibre.

$$\theta = V\ I$$

The Verdet constant (or Faraday Effect) of silica fibres decreases as the wavelength of the light beam increases. Nevertheless we propose to operate the fibre current sensor in the low sensitivity region (1.3-1.5µm) because at these wavelengths we reduce the effect of radiation (defaults in fibers, darken the fiber, etc.) and the light source are commercially available.
The influence of temperature on the Verdet constant from room temperature to 77K has been investigated (figure 9).

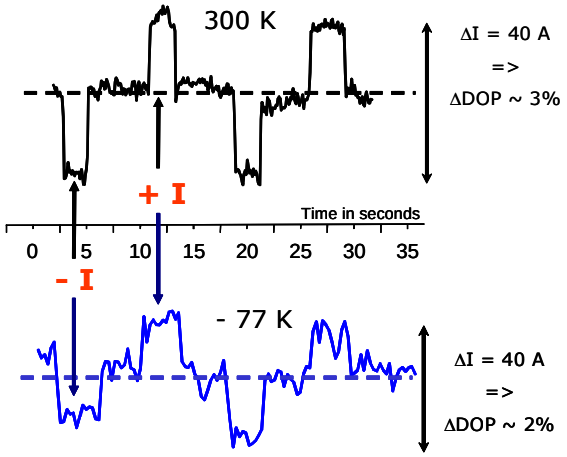

Figure 9: FOCS sensitivity when they are submitted to low temperature (77K, liquid nitrogen)
[Data from B. Brichard SCK.CEN ITPA meeting 2006]

Comparing data at room temperature and 77K shows that from the same current in the conductor, the Faraday rotation is smaller at 77K, the signal is noisier and the time response appears to be slightly bigger. Taking into account the FOCS behaviour at low temperature, 77K (enhanced Radiation Induced Absorption effects and low Verdet constant) it seems important to favour operation at high temperature (typically 120°C). It means that our efforts should focus on the installation of the sensors on the 2nd skin of the vacuum vessel along the ex-vessel tangential and radial coils.
Using the model developed for the Rogowski the phase shift due to the magnetic field has been estimated (figure 10) for the standard scenario. On the flat top of plasma current, the Faraday rotation amplitude is bigger than 2 turns. It means that the electronic system will have to take into account phase jump in case of fast current variation.

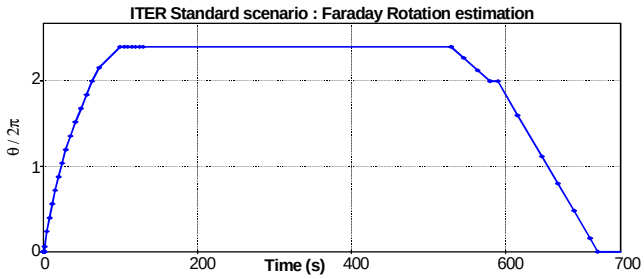

Figure 10: Calculation of the FOCS Faraday rotation amplitude during ITER standard scenario ($V=10^{-6}$ °/T m

CONCLUSIONS

Three kinds of ITER magnetic sensors have been reviewed. The ex-vessel coils design has been modified to obtain coils with an effective area of $2m^2$. The equilibrium reconstruction accuracy has been assessed using the code EFIT. Various types of error were investigated showing that robust equilibrium reconstruction can be obtain by combining the whole set of magnetic sensors (in-vessel coils, flux loops and ex-vessel coils). The considered errors (offset of 10mT and error of 5%) lead to gap errors lower than ITER specifications but using only the ex-vessel coils to reconstruct the equilibrium produced not acceptable errors.
The Rogowski design has evolved to incorporate fibre optic current sensors. 3D modelling and simulation based on current loops principle have been performed. Small winding defaults have been modelled. They could account for joints or irregular winding. From the simulation one conclude that putting joint at the top and at the bottom of the TFC introduces errors which are compatible with ITER requirement.
Fibre optic current sensors have been considered. Low temperature enhances the Radiation Induced Absorption effect due to neutrons and the Verdet constant become negligible. Therefore we should focus on the installation of such sensors in higher temperature places, for example on the 2nd skin of the vacuum vessel.

REFERENCES

[1] Assessment of the conceptual design for in-vessel magnetics. E. Coccorese et al. (ENEA-CREATE, Italy), Final Report of EFDA Contract 00-571 2001

[2] Failure mode analysis of the ITER magnetics diagnostic system, carried out under EFDA Contract 02-1001 (ENEA-CREATE, Italy)

[3] Re-evaluate and optimize the sub-system for measuring halo currents, carried out under EFDA Contract 02-1000 (ENEA-RFX Padova, Italy)

[4] Ph. Moreau, P. Defrasne, Final Report on ITER magnetics diagnostic design study EFDA contract 04-1206 Part 1: Outer vessel tangential and normal coils

[5] KUZNETSOV, Yu.K., et al., Sov. J. Plasma Phys. 13 (1987) 75

[6] F.C. Morabito Failure mode analysis of the ITER magnetics diagnostic system, carried out under EFDA Contract 02-1001 (ENEA-CREATE, Italy)

[7] J. How. Project Integration Document (PID) ITER_D_2234RH. Realise 2.0 September 2005

[8] J.M. Moret et al. Final Report on ITER magnetics diagnostic design study EFDA contract 05-1345

[9] Design Description Document: DDD 11 "Magnet Section 1. Engineering Description" September 2004

REPORTS AND PUBLICATIONS

- Final Report Contract EFDA 05-1343 Part I ITER magnetics diagnostic design study: Ex-vessel normal and radial coils DIAG/NTT-2005.035
- Final Report Contract EFDA 05-1343 Part II ITER magnetics diagnostic design study: Ex-vessel continuous Rogowski DIAG/NTT-2005.036
- Final Report Contract EFDA 05-1343 Part III. ITER mag. diagnostic design study: Ex-vessel Fiber Optic current sensor DIAG/NTT-2005.037

TASK LEADER

Philippe MOREAU

DSM/DRFC/STEP/GPAS
CEA-Cadarache
F-13108 Saint-Paul-lez-Durance Cedex

Tel. : 33 4 42 25 36 39
Fax : 33 4 42 25 26 61

e-mail :philippe.jacques.moreau@cea.fr

CEFDA05-1343PI

Task Title: TW5-TPDS-DIASUP1: DIAGNOSTIC DESIGN FOR ITER: PORT INTEGRATION

INTRODUCTION

ITER requires an extensive set of diagnostic systems to provide several key functions such as protection of the device, input to plasma control systems and evaluation of the plasma performance. These diagnostic systems are to be integrated inside the vacuum vessel of ITER by means of water cooled stainless steel structure (42t, 2m x 2m x 3m) named port plug structure. The port plug structure must perform basic functions such as providing neutron and gamma shielding, supporting the first wall armour and shielding blanket material, closing the vacuum vessel ports, supporting the diagnostic equipment.
In 2005 Euratom-CEA Association contributed to general, structural and thermal analysis [1], those assessment focused mainly on the equatorial port plug EQ#01 (see figure 1) chosen as representative. These detailed analyses have highlighted some design issues which were worked out through different solutions.

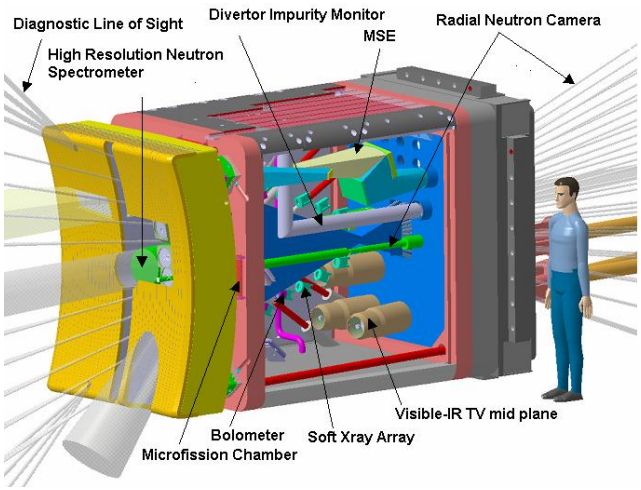

Figure 1: View of the equatorial port plug Eq#01 and associated diagnostics

These engineering activities have been pursued during 2006. They concerned the validation of a new reference design of the port plug structure and specific design options, in parallel wider activities have also been assessed [2].

2006 ACTIVITIES

The different tasks to be done are divided into 2 types of activities: engineering activities (including CAD effort) and "other activities":

- The engineering activities essentially consist of finite lements analysis of the mechanical and thermal behaviour of the port plug in order to validate a new design. Associated CAD activities are performed in order to improve the design of some specific parts of the port plug (as the Blanket Shield Module attachment system, or the far forward extension module), and in studying the handlings of some pieces (port plug structure, window plate, tubes…).

- The "other activities" are wider activities like, remote handling, risk analysis, review of specifications, manufacturing processes and quality control associated, prototyping and R&D activities. These tasks have been partly done by CEA, and by an industrial subcontractor of CEA. They constitute a first approach on each topic and will provide inputs for the continuation of the port plug activities to be done in the frame of future contracts.

ENGINEERING ACTIVITIES

Port plug mechanical behaviour
A number of changes have been made to the port plug design. The top beam in the latest design now consists of one top plate rather than three distinct pieces, this element is still dowelled and bolted to the side of the port plug in which the design of a labyrinth has been done to reduce neutron streaming. Another proposed change is to remove the front plate of the port plug structure which is now formed by the front shield module (see figure 2).

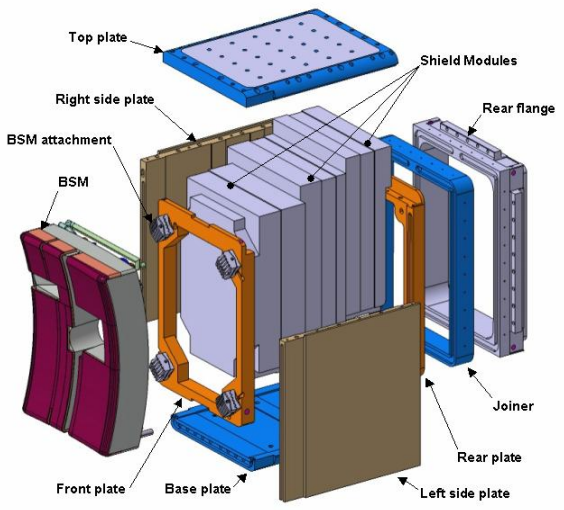

Figure 2: New reference design of the Equatorial port plug

The purpose of this mechanical assessment is to validate the mechanical behaviour of this new design under the new mechanical electromagnetic reference case of load MD40ms (major disruption of 40 ms duration, radial torque of 4.43MN.m). Some particular design optimisation such as the BSM attachment system and the bolting of the top plate have also be considered.

In order to decrease the maximal stresses in the vicinity of the attaching bolts and pins of the top plate, another study has been realized by changing the quantity and the distribution of bolts and pins. In the original model, there were 12 bolts and 21 pins, by putting only 3 pins at the front fixation and 5 pins at the rear fixation and having only bolts on the side fixation, the study shows that the torsional stiffness of the port plug is not changed (maximal displacement of 1.35mm), whereas the maximal stresses highly decrease (the maximal stresses reach locally 230MPa, instead of 500MPa with the previous configuration). This leads to a total number of bolts of 8 and a total number of pins of 20.

The requirements concerning the BSM attachment system can be summarized in one sentence: “provide a rigid, stable, self aligning and self preloaded, minimally sized, non-cooled mount for the BSM". It also has to be simple, reliable and dismountable by remote handling. To improve and mostly simplify the initial design (gimbal principle), alternative solutions have been studied, based on V-shape supports (see figure 3), key-locked by shear pins, and ensuring natural and simple contacts between the BSM and the front plate.

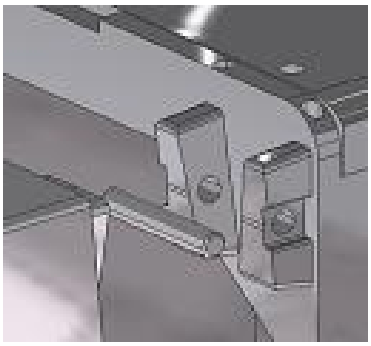

Figure 3: V-shape BSM attachment system

This design has been improved by running mechanical and thermal analyses towards an optimized solution, with high mechanical stiffness and thermal performances. The basic design of the V-shape solution has showed that fairly rigid supports permit to avoid high stresses in the pins (but localized on the BSM and supports bore diameters), whereas too rigid supports concentrates the shearing efforts on the pins, over the acceptable limit. The solution chosen for later studies is the “optimized with cylindrical pins”, the stress results associated to this solution are summarized on figure 4.

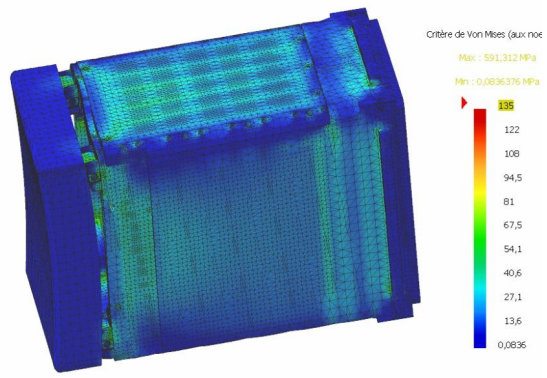

Figure 4: Stresses on the port plug with V-shaped BSM attachments

Port plug thermal behaviour

The objective of this study is to determine the thermal behaviour of the equatorial port plug taking into consideration the updated mechanical design of the structure and the new configuration of the coolant circuit.

The thermal load applied to the port plug is a specific heat generation due to the neutron radiation comprised between 600000W.m^{-3} on the front plate and 165000W.m^{-3} on the bolting flange.

For the transient calculations, the heat load is supposed to be applied during 3000 seconds and to be equal to 0 during the following 3000 seconds. The temporal evolution of the maximal temperature (in the BSM attachment, see figure 5) shows that the equilibrium is reached after 2 cycles, and that the maximal temperature is almost identical to the one obtained in steady state analysis (437 °C). This result shows that for preliminary design, steady state calculations give good results, and thus can be considered sufficiently accurate at this phase.

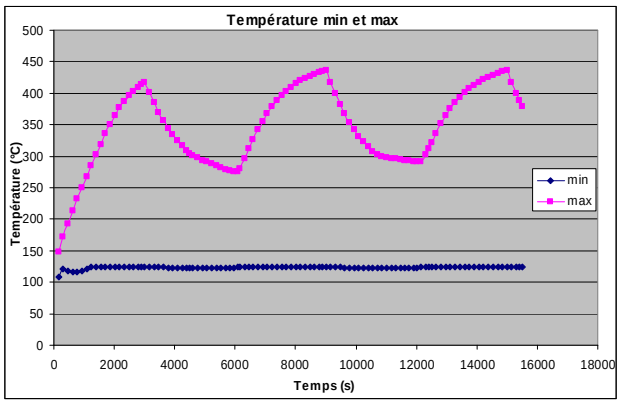

Figure 5: Temporal evolution of the maximal temperature

Secondary stress (thermal stress) is under 50MPa on most of the port plug, and the reduction of the cooling system did not induce a real difference in thermal stress in the rear parts of the port plug. Unsurprisingly, the high stress areas are concentrated in the front plate and BSM attachment (see figure 6): 500MPa in the front plate, near cooling pipes (thin material between pipes and the front of the plate), 450MPa in BSM attachments, 750MPa near the attachments pins.

Some extremely severe stresses appear in some very small areas. They are caused by geometry problems (sharp angles).

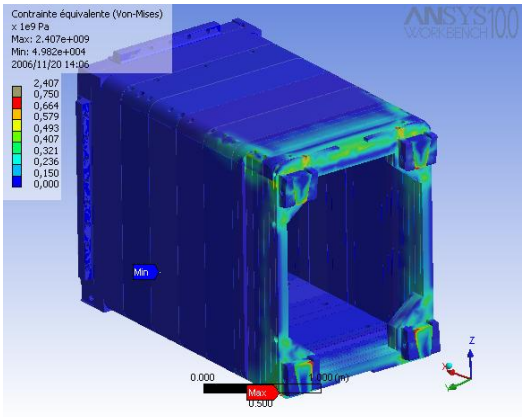

Figure 6: Thermal stress

The cooling system used in this calculation was optimised for thermal response of the port plug, and this is why some areas near cooling pipes show high stress values. An optimisation on the distance between the pipes and the front of the front plate on both thermal and thermo-mechanical aspects will certainly allow us to reach lower stress values without too high temperatures.

Preliminary study of visible IRTV diagnostic module extension

The objective of this study is to design, with respect to the thermal and mechanical loads to which it is subject to, the far forward diagnostic module extension, a component located between the BSM and the first shield module. The main function of this far forward extension is to support a part of the visible IRTV diagnostic, which has several mirrors close to the plasma in this area (see figure 7). The proposed design consists in a compact module to limit the size of the aperture in the BSM and thus limit the loss of shielding due to this aperture. This component will use the first wall BSM technology made up of a layer of copper and a layer of beryllium. Due to the great heat loads applied to the module extension, all the components (module, first wall and 2nd optical head mirrors) have to be actively cooled. Moreover, a shield module will have to be put inside the hollow part of the module to ensure the shielding function of the port plug components which are located after the BSM.

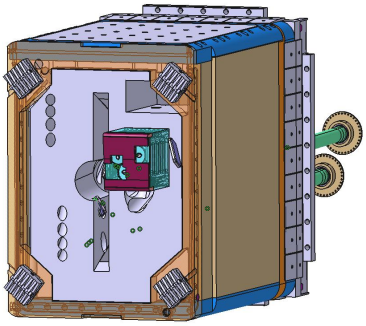

Figure 7: Proposed design of the far forward module extension

Both thermal loads (nuclear heating of 11MW.m^{-3}, plasma heat flux of 0.5MW.m^{-2}) and mechanical loads (radial moment of 1MN.m for all the module, vertical force of 1600 kN.m^{-3} radial force of 4300 kN.m^{-3}) have been applied to this component.

With these conditions and this preliminary design, thermal can be validated for the majority of the far forward module extension (with small zone in the front face where temperatures are higher than 400°C). Concerning mechanical, the design done to resist the radial moment is not completely optimized yet. This optimisation could consist in adding stainless steel on the critical zones like the sides of the far forward module extension. However, an optimisation of a design for both the thermal and mechanical loads has to be done.

OTHER ACTIVITIES

Diagnostic port plugs remote handling approach

The maintenance of ITER is strongly constraints by the levels of irradiation induced by the action of the neutron streaming and by the presence of beryllium and tritium in the vessel. These are the reasons why the maintenance cannot be done classically and why the remote handling is crucial. For all the components of the first wall, the strategy is to make the refurbishment in hot cells. This means that a transfer phase is necessary. The main difficulty is that all in vessel components must be confined during their transport to prevent from beryllium dust or tritium contamination. This induces that even if the transfer preparation can be made hands-on, all the transfer and refurbishment tasks must be done in full remote handling, and the transfer cask must be equipped with a double door system (see figure 8).

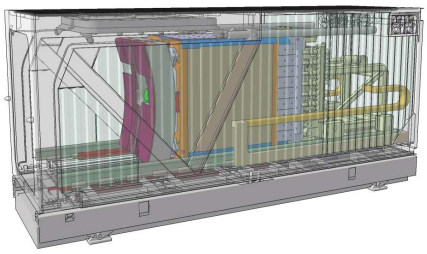

Figure 8: View of the Transfer Cask

This transfer equipment is composed of 4 main sub-systems:

The Cask Container: tight but not shielded, designed to contain the port plug plus the whole equipment needed to handle it.

The air cushion system: the cask is remotely controlled and the gravity load is supported by making floating the cask on an air cushion.

The double door system: common to all kind of transfer casks, it ensures the continuity of the sealing to the contamination.

The port plug mover: able to carry the port plug components in cantilever from its location in-vessel to the inside of the cask. Two degrees of freedom allow fitting the position and orientation of the component during its stroke. These displacements are provided by hydraulic power and controlled by the mean of force sensors. A frame mounted on the gripper is equipped with screwing/unscrewing devices.

The different necessary tools and equipments of the hot cells will be of different nature: diagnostic inspection tools, heavy remote handling and end-effectors, force feedback remote handling and end-effectors, automatic processes, test and conditioning equipments, spare parts.

The maintenance of the diagnostic port plugs is an operation that will certainly occur several times in the reactor's life. The sequence of preparing the port cell, transferring the components and refurbish them in the hot cells must be very efficient in order to provide the optimal availability of the tokamak. The design of the diagnostic port plugs must be carried out by considering as a priority this technical constraint and working closely with the remote handling team. This is especially true for the hot cell layout and equipment that will have to fit all the specific needs of the diagnostic port plug refurbishment.

Review of specifications, quality assurance, manufacturing and prototyping

These tasks have been studied jointly with a CEA industrial subcontractor specialized in nuclear environment.

The port plug specifications document established by ITER Team has been revisited in order to make it more concise and moreover conform to nuclear components specificities.
It appears necessary to implement a quality management system as soon as possible which will have to meet the requirements of the 10th August 1984 French decree relative to quality for nuclear facilities and/or the AIEA safety standards n°50 C/SG-Q "Quality Assurance for Safety in Nuclear Power Plants and Other Nuclear Installations, Codes and Safety Guides Q1-Q14".
A quality plan will have to be established in order to be submitted to the potential suppliers, and will be completed by the contractor's manufacturing plan. This plan will indicate the break and inspection points required for technical reasons (critical manufacturing steps as control of welding), and for administrative reasons (control of French regulation, ILE…).
Because of their location inside the vacuum vessel and thus in a nuclear environment, the design and manufacturing of the port plug components will have to respect specific construction codes and standards. For the port plug structure, which is SIC classified due to its role of first containment barrier at the vacuum vessel port, and which is submitted to severe mechanical and thermal loads (risk of creeping), it is suggested to use the same code as for the vacuum vessel (RCC-MR Class 2). The cooling system is assumed to be SIC due to its role of removal of nuclear power, and of transport of activation and corrosion products through cooling water. So the suggestion is to use the ASME code, or the RCC-MR Class 2 (for homogeneity reasons). For the shielding modules, which only have a role of passive shielding, a construction code should not be required.
The critical points of the port plug manufacturing are the welding of important thickness (up to 140 mm) and the deep drilling for the cooling channels. The choice of the process will depend on the potential manufacturers availability, the relevance of the process regarding construction code and the cost. The best welding process choice seems to be the electron beam welding since it is a proven technology. As deep drilling is also a proven technology, it is suggested to use this solution as reference, and to examine the possibility to perform R&D activities on the HIP process.
The aims of prototyping in a nuclear facility are to check the performance requirements and to check the safety requirements. Concerning performance, the suggestion is to qualify items which could induce delay, or having an important risk of non compliance. For safety purpose the suggestion is to qualify items having a role in containment barrier and shielding.

Risk analysis
The port plug project is at the very beginning so most of the risks could concern programmatic, organizational aspects and communication in an international context. Today the most obvious risk concerning the technical aspect could be the difficulty to obtain the good reference information to perform engineering actions.
On the basis of this first approach our Association could propose to put in application risk management process in the frame of the 2007 contract.

CONCLUSIONS

Performed analysis such as CAD, mechanical and thermal studies validate the new version of the equatorial port plug structure, including the design integration of the far forward diagnostic module extension containing the first set of the visible IR TV mirrors. The mechanical behaviour of the port plug cantilevered model has been validated and two optimizations are proposed concerning the top plate fixation and the BSM attachments (V-shaped solution).

Thermal transient and steady state analyses have been performed and showed steady state analyses is sufficient for preliminary design. Most of the port plug reaches acceptable temperature, which allows us to reduce the cooling system in certain parts. Nevertheless, temperatures and thermal gradient in the front plate and the BSM attachments are quite high (390 and 450°C, several hundred degrees Celsius variation in a few centimetres) and remain to be optimised due to the induced secondary stresses.

Additional tasks such as risk analysis, remote handling, and collaboration with a company specialized in nuclear engineering have been performed. At the light of those activities which need to be pursued next year some design considerations will have to be addressed.

REFERENCES

[1] L. Doceul, 'Final report on diagnostic design for ITER port integration (EFDA Contract 04-1206)', PEFC/NTT-2005.014 Rev. 1 January 2007

REPORTS AND PUBLICATIONS

[2] S. Salasca, 'Engineering assessment of diagnostic port integration on ITER, Final Report (EFDA Contract 05-1343 D1.2)', PEFC/NTT-2006.023 Rev. 0 November 2006

TASK LEADER

Louis DOCEUL

DSM/DRFC/SIPP/GIPM
CEA-Cadarache
F-13108 Saint-Paul-Lez-Durance Cedex

Tel. : 33 4 42 25 61 65
Fax : 33 4 42 25 49 90

e-mail : louis.doceul@cea.fr

CEFDA05-1343TH

Task Title: TW5-TPDS-DIASUP1: DIAGNOSTIC DESIGN FOR ITER: THERMOCOUPLES DIAGNOSTIC

INTRODUCTION

Thermocouples on first wall components will be used in ITER for machine protection, and also they can be used for calibration purposes of the IR/VIS diagnostic. The objectives of the present study are:

- Review the currently foreseen implementation of the thermocouple diagnostic on ITER. In particular, consider suitable types of sensors, the cabling needs, integration of sensors and cables in ITER, remote-handling aspects and, if relevant, calibration issues. Define integration requirements, including spatial requirements, cables and connectors. Assess the measurement performance that can be expected in relation to the ITER measurements requirements,
- Assess the requirements and implementation of thermocouples for other purposes such as for calorimetry, and optimized for cross-calibration of divertor thermography,
- Propose a comprehensive outline plan for the full implementation of the thermocouple diagnostics on ITER, incluse identification of critical issues and questions that need to be resolved, and detailed specifications for future design tasks on the system,
- Assess existing documentation and assist ITER IT in the updating of ITER documentation in this area. Support the ITER IT in the writing of procurement specifications for the diagnostic procurement packages.

2006 ACTIVITIES

PREVIOUS STATUS OF THE THERMOCOUPLE DIAGNOSTIC

The measurement of surface and body temperatures in the high heat flux components of the divertor (inner and outer targets) and of the blankets are required. They will be used as reference for the visible/IR TV system and possibly to derive the heat flux on these components.
In the initial specifications, Thermocouples will be used to measure the surface temperature within the range 200°C to 1500°C with an accuracy of 20°C. Some platinum resistance temperature sensors can be used for calibration of thermocouples. Temperature measurements will be used during the operation for the monitoring of plasma facing components (blanket shield modules on port plugs, blanket modules and divertor cassette surfaces) in complement to the IR, and visible/IR TV diagnostic.
A total of about 1000 thermocouples are foreseen to be implemented on the in-vessel components, following the distribution presented in figure 1.

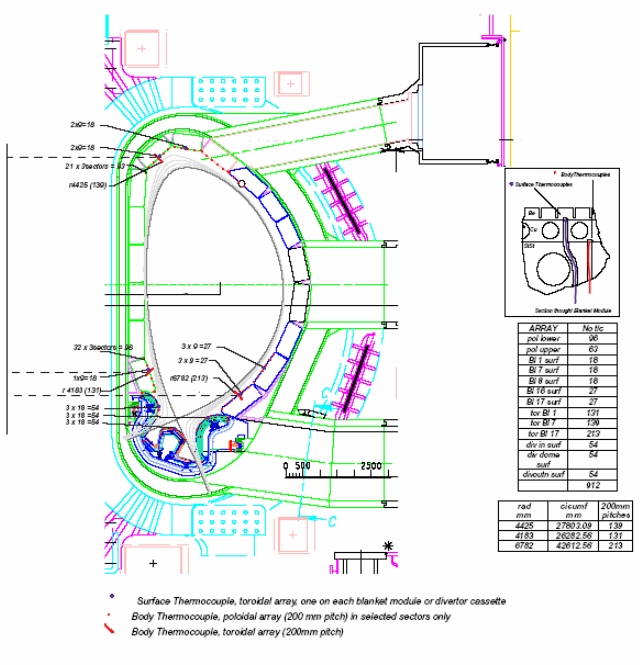

Figure 1: Location of temperature sensors in blankets modules and divertor

Blanket: Blanket instrumentation is combined with the IR Viewing systems to keep the number of both systems to an optimum minimum. Generally only the blanket modules in the limiter region and at the top of the Torus are instrumented with thermocouples. At selected positions there are more complete thermocouple arrays. With ~200 mm spacing there are up to 13 thermocouples on some of these modules.
This visible/IR TV diagnostic will be made of two wide-angle camera systems which will give views of the first wall and parts of the divertor in the IR and visible wavelength ranges. The wide-angle viewing systems will be located in the upper ports #02, #05, #08, #11, #14. It is expected that combining several cameras can achieve high coverage of the area of the first wall (80% Assessment based on preliminary analysis for ITER-98).
The thermocouple arrays are situated as near as possible to the blanket surface to act as suitable calibration measurements for the IR cameras. It is expected that there will be losses of these signals as the wall of ITER is progressively irradiated. Individual reference thermocouples allow for no redundancy, consequently they are more deeply buried in the Blanket Module. The electrical connection of the Blanket Thermocouples is made during the installation of the blanket modules. An electrical connector is provided on the back plate and wires are routed to the nearest diagnostic poloidal cable conduit.
Divertor: The basic idea for the location of TC diagnostic is to have a toroidal distribution as evenly as possible. Cassettes with TC diagnostics are located at places that can be accessed by the remote handling ports (#2 and 14)

on instrumented cassettes. These are standard cassettes modified to incorporate special sensors and wiring mounted on cassette sides, while allowing remote installation in the same way as for standard cassettes. Instrumented cassettes are either side of diagnostic cassette. The location of the thermocouples proposed is given in figure 2, using the mounting principle outline given in figure 3.

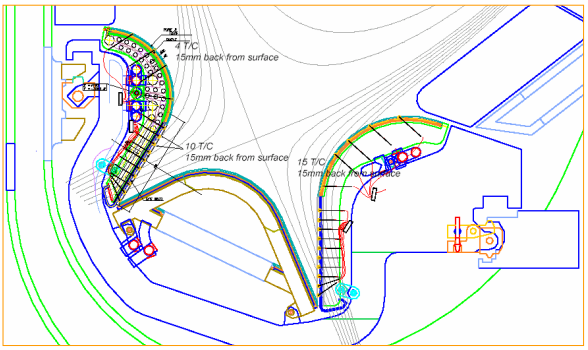

Figure 2: Location of the Thermocouples on the divertor

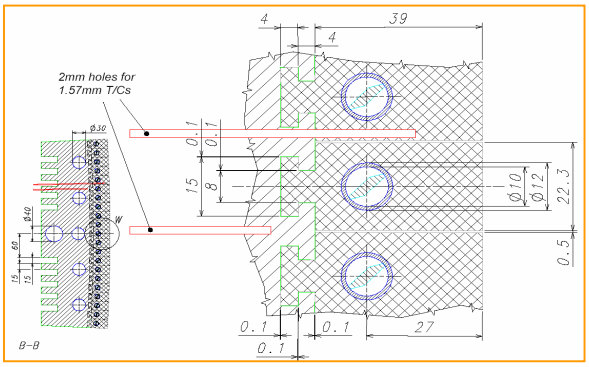

Figure 3: Thermocouples mounting principle in the divertor

Table 1 presents a summary of the thermocouple diagnostic as proposed, corresponding to a total amount of 150 TC located in the vacuum vessel.

Table 1

		number of sensors	Comments
Divertor			
Port #2	Cassette#3 or cassette #5	Thermocouples Inner (x 14) and Outer (x 15)	
Port #14	Cassette#39 or cassette #41	Thermocouples Inner (x 14) and Outer (x 15)	IR thermography is located at Port #16
Blanket			
Inboard	Port #1,2, 3, 5, 8, 9, 11, 14,17	4 Thermocouples at each port	G01 : Vis/IR TV diagnostic 80% coverage of the inner first wall
Outboard	Port #1 (x3), 4 (x6), 10(x6), 16 (x6)		

TEMPERATURE SENSORS OPERATING CONDITIONS

In order to choose the most appropriate temperature sensors type, the geometries of the components and the maximum temperature at the point of measurements are needed.

Divertor

Two main load cases conditions are considered among those presented in the Divertor DDD:

- Case I: ''Steady state'' semi-detached plasma : It is assumed that 30% of the incoming power is dissipated through radiative mechanisms and that 70% is conducted to the lower section of the target, with a maximum heat flux of 10 MWm^{-2} .
- Case II: ''Steady state'' attached plasma (slow transients). All the thermal power is conducted to the lower section of the inner and outer vertical targets; a small fraction of the power is radiated to the other surfaces, with a maximum heat flux of 20 MWm^{-2}.

The maximum temperature values computed with the CEA CASTEM finite element code for a CFC monoblock for an incident heat flux of 10 and 20 MWm^{-2} are respectively 1190°C and 2500°C. The temperature gradient is roughly 200°C/mm in the central part of the monoblock.
In addition, following, for the nominal 500 MW fusion power, the peak neutron wall loading in the divertor region is 12 MWm^{-2}. The peak wall loading values in the inner and outer vertical targets are 6 and 9 MWm^{-2} respectively. The dpa on carbon tiles of the vertical target is 1.2 at maximum for 1-year full irradiation time.
In addition, the armour materials (CFC for the vertical targets and W for all other plasma-facing surfaces of the divertor) will be eroded during the discharges. They have been selected to fulfil the goals of sustaining 3000 full power discharges of 400s duration, with one in ten discharges ending in a disruption and with a frequency of one high power transient per ten discharges, that occur when the SOL is fully attached to the target. Therefore, the temperature sensor cannot be implemented close to the surface receiving power, if it has to survive the lifetime of the divertor (10 mm for the CFC, and 7mm for the W).

Blanket

The blanket consists of a shield body on which a first wall (FW) is mounted. The cross-section of the FW panel at penetration holes is presented in figure 4. The heat and neutron loads on the first wall are presented in table 2.

Table 2: Loads on blanket FW

	Value
Heat flux on first wall Steady-state, average/max (MWm^{-2}) Transient up to 10s, max (MWm^{-2})	 0.25/0.5 05-1.4
Neutron wall loading Steady-state, average/max (MWm^{-2})	 0.55/0.78
Neutron fluence, average/target max (Mwa/m^2)	 0.3/0.5
Volumetric heat deposition in Be (MW/m^3)	 4.79

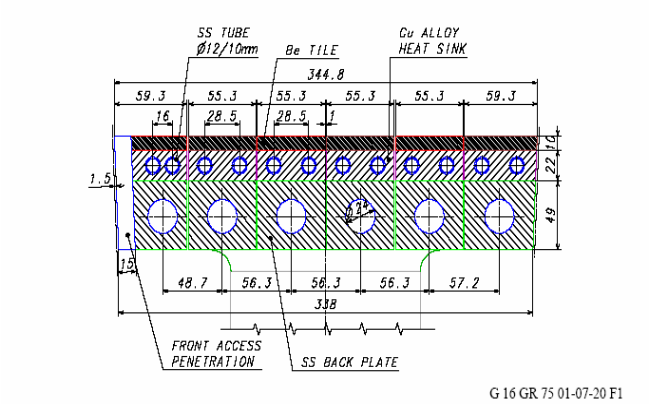

Figure 4: Cross section of the FW pannel

The maximum temperature values and peak neutron damage for the different blanket materials have been computed, they are respectively:

- 300°C and 1.6 dpa in the Be armour
- 220°C and 5.3 dpa in the CuCrZr heat sink
- 220°C and 2.7 dpa in the SS 316L structure

POTENTIAL TEMPERATURE SENSORS

For the selection of potential temperature sensors, the operating temperature range is important, but also their behaviour in the ITER nuclear environment. In addition, for the temperature measurements in a component, the size of the sensor is an important parameter. The sensor may modify the temperature field locally and lead to a wrong measurement. Thermocouples are preferable for this type of measurement.
Type K or N Thermocouples can be used for the blankets and probably for the most interior sensors in the divertor. For the sensors located close to the divertor target surface C type thermocouples are required.
As the upper temperature limits and life expectancy of all the thermocouples are dependent on wire size, it seems convenient to use sheathed sensors with 1.5 or 2 mm outer diameter.
To set the thermocouples in a Plasma Facing Component, a method commonly used, is to bore a hole in the material in which the thermocouple is inserted. A radial gap of 0.05 to 0.1 mm is made between the sheath and the material.. An adhesive adapted for high temperatures operation is used to glue the thermocouple sheath at the hole base. Commercial products are available on the market for operation at temperatures up to 2000°C. This type of adhesive has been already used successfully in different materials (CFC, W or CuCrZr).

POTENTIAL METHODS FOR THE ANALYSIS OF MEASUREMENTS

The surface temperature of a component can theoretically be measured with the IR diagnostic. Nevertheless the calibration of the transmission line is required and, for this purpose, the temperature of the target has to be measured accurately. One issue comes from the fact that the calibration is usually performed during the bake-up phase, during which the temperature of the component is lower than that reached in plasma and may be out of the range of the IR diagnostic.
If we use a PFC as the target, some error may appear. It may be due to deposits on the surface. The IR system measures a temperature which is not representative of the component surface. This depends on the IR emissivity of the deposit, on its mass and on its thermal connexion to the component surface. During the discharges, PFC located in deposition zones will be facing this problem, while those located in eroded zone should not be concerned. TC should be located in zones with erosion instead of deposition.
The other issue is the derivation of the trace of the heat flux level and profile at the PFC surface during pulses. With the restrictions mentioned above, the IR diagnostic can be useful to derive at least the heat flux profile. The use of TCs to measure the temperature inside the component is complementary to the IR measurement in order to derive the heat flux level.
At JET, a technique based on the TCs data and on thermal finite elements simulations, has been developed to derive the power deposition profiles on the MkIIGB divertor.
An other technique, based on the deconvolution of the temperature measurements traces and of a 2D impulse response of the tile may be applied to reconstruct the trace of the heat flux. 2D calculation is required because of the anisotropy of the CFC. The impulse response is calculated with the thermal quadrupole method. A regularization is required for the inverse problem. The IR frames are used to assess the spatial heat profile at the surface of the plasma facing component.
Even if presently this technique is not yet fully validated on the JET divertor data, the present results are promising.

POTENTIAL USE OF TEMPERATURE SENSORS TO DERIVE THE NEUTRON POWER ON THE BLANKETS

The use of thermometers (temperature sensors) on the blanket module cooling lines to derive the neutron power generated in the first wall (FW) panels and in the shield blocks (SB) on which the FW is mounted has been proposed previously.
The basic idea is that, if we can measure with the bolometry diagnostic the radiative power falling on the surface of FW, we could use calorimetric measurements on the cooling pipes feeding the FW and BS elements to derive the neutron power generated in these elements. The location of the temperature sensors required to do these measurements are presented in figure 5.

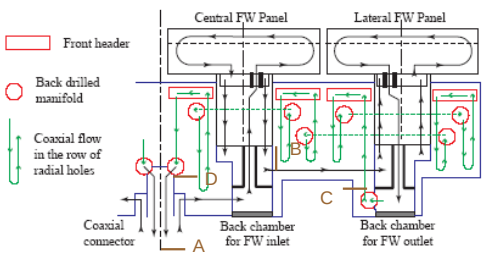

Figure 5: Temperature sensors in the blankets

PROPOSAL FOR THE THERMOCOUPLE DIAGNOSTIC LAY-OUT

K or N Type thermocouples can be used in the ITER operating conditions except for the temperature measurements close to the surface of the divertor vertical target which receives the heat flux. In this last case, C type Thermocouples will be required.
The diameter of the TC sheath will be ideally 1.5 to 2 mm. The outline of the TC is presented in figure 6.

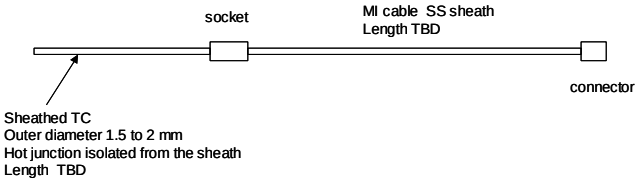

Figure 6: TC outline

The intermediate socket is in fact a metal piece in which the sheath of the TC and that of the MI cable are welded. Vacuum tightness is required for this connection. The cable wires between the socket and the connector of the feed-through will be made of the same materials as that of the thermocouple. The end connector must be compatible with the linking plug located behind the divertor cassette. It must be compatible with a Remote handling operation. It is presently not defined. For the blankets, the end connector must be compatible with the feed-throughs selected for ITER.

Divertor TC Diagnostic

For the lower part of the vertical target, the thermocouples will be imbedded in the CFC mono-blocks at 10 to 15 mm from the surface and possibly parallel to the iso-temperature surfaces. The TC is ideally located at the center of the monoblock parallelly to the surface receiving the flux (figure 7).

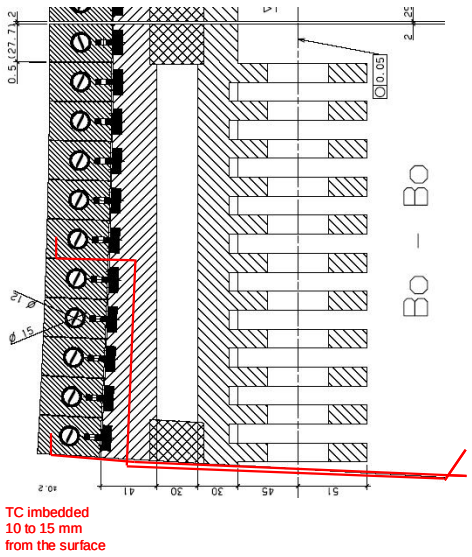

Figure 7: Location of TC in divertor CFC monoblocks

CONCLUSIONS

At the end of this phase, the principle of the temperature measurement diagnostic in the blanket and divertor of ITER has been defined.
A technique based on the measurement of temperature inside the first wall material associated with an analysis method based on the deconvolution of the TC trace is proposed. This promising technique is under development but it has to be validated on the configuration of the blankets and divertor of ITER. Simulated results obtained by ANSYS simulations can be used to do this analysis.

Some questions need further work:

- Definition of the sensor from the thermocouple element to the outer connector. This work must be done in close contact with potential manufacturers taking into account ITER component specifications for connectors and feed-throughs. Prototypes are required.

- Definition and test of the TC implementation technique. Techniques have been identified, but they have to be validated before their use in ITER. A development programme is required. The implementation of TC prototypes in Tore Supra actively cooled Plasma facing components such as the Toroidal Pumped Limiter can be imagined to check the complete thermocouple diagnostic design. The collected data, could be used to improve and validate the analysis methods.

REPORTS AND PUBLICATIONS

[1] Diagnostic design for ITER Final Report EFDA contract/05-1343/Thermocouples

TASK LEADER

Michel CHANTANT

DSM/DRFC/STEP/GARV
CEA-Cadarache
F-13108 Saint-Paul-Lez-Durance Cedex

Tel. : 33 4 42 25 49 80
Fax : 33 4 42 25 44 21

e-mail : michel.chantant@cea.fr

TW5-TPDC-IRRCER-D03

Task Title: ASSESSMENT OF IR FIBRES FOR THERMOGRAPHY APPLICATIONS, INITIAL GAMMA INDUCED EFFECTS, THEN NEUTRON IRRADIATIONS - FIBRE SELECTION AND PROVISION, DIAGNOSTIC PREPARATION AND MEASUREMENTS

INTRODUCTION

In the course of the development of a concept for a spectrally resolving thermography diagnostic for the ITER divertor using optical fibres [1] irradiation tests of optical fibres for the infrared range are being carried out in a collaboration between the Euratom-CEA association and the SCK-CEN Mol association (Belgium).

2006 ACTIVITES

The performance of the proposed ITER diagnostic system had been analysed [1] in the range from 1 to 10 µm and sufficient performance is expected in the 2-6 µm window. Silica fibres which are relatively radiation hard in the near infrared (NIR) range are only transparent up to 2 µm. In Tore Supra, were used with success ZrF_4 fibres transparent up to 4 µm [2], but too little was known about the radiation hardness of these fibres. They became therefore the prime candidate to investigate in our first irradiation tests. We selected ZrF_4 fibres from Reflex analytical of 3.33 m length and two types of fibre from Le Verre Fluoré named IR Guide 1 (ZrF_4) and IR Guide 2 (HfF_4) of 2 m length. Hollow fibres which are made of silica capillaries with an internal coating of a metal and a dielectric can be transparent from about 2 µm to beyond 10 µm. This fibre type promised a certain radiation hardness and a particular potential [3] for active thermogarphy measurements. Therefore 2 hollow fibres from Polymicro with internal Ag/AgI coating, 750 µm internal diameter of a length of 2 m and 8 m were also selected for the first radiation tests. The total length of a potential fibre path in ITER from the pumping port of the divertor cassette to the bioshield is about 8.6 m. Over this length the dose rate of neutrons of an energy > 0.1 MeV at full power operation decreases exponentially from 10^{17}n/m²s at the port to $0.5 \cdot 10^{14}$ n/m²s at the bioshield with a caracteristic decay length of 1.6 m [1]. The full lifetime dose of ITER (7600 hours of full power operation assumed) at the potential fibre connection point at the cassette is $3 \cdot 10^{23}$ n/m². The ratio of γ dose rate to neutron (> 0.1 MeV) dose rate in ITER is typically of the order of [4] 1 Gy/s for 10^{15} n/m²s. This means that the full lifetime γ dose is expected to be 300 MGy at the transition from the divertor cassette to the divertor port and 150 kGy at the bioshield. For an initial test of IR fibres we planned γ irradiaton in the multi kGy range with spectrally resolved in-situ measurements troughout the irradition period and the subsequent period of time without irradition to investigate both the loss and the recovery of transmission. The measurement setup we used has been described in the 2005 CEA Technofusion report. We carried out gamma irradiations using the Co^{60} irradiation facility RITA of the SCK-CEN Mol at a maximum dose-rate of 0.42 Gy/s up to a total dose of about 5000 Gy. We observed that the optical transmission of ZrF_4 fibres strongly decreased, primarily for wavelengths below 2 µm (figure 1).

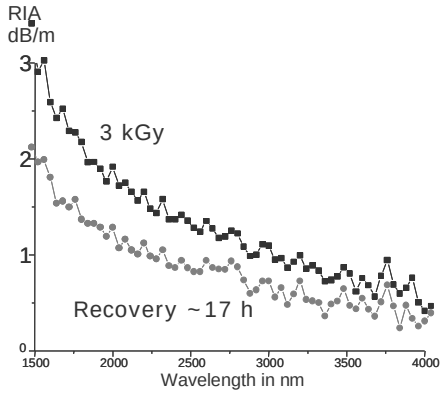

Figure 1: Spectral distribution of radiation induced attenuation (RIA) on ZrF4 fibre (Ir Guide 1 from Le Verre Fluoré)

In this type of fibre typical optical losses can reach 50 % at 5 kGy around 3 µm. Nevertheless, the optical transmission can be significantly recovered by thermal annealing at room temperature (figure 2) or more rapidly by performing a thermal annealing treatment at a temperature of 100°C (figure 3). These results were independent from the manufacturer of the fibre.

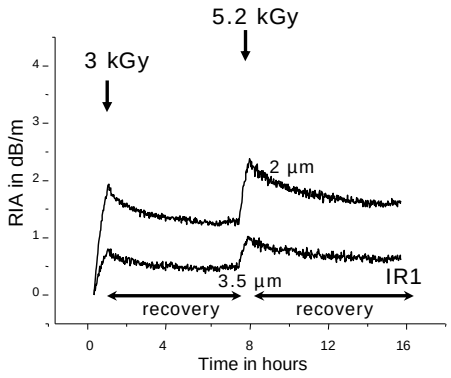

Figure 2: Evolution of RIA at two wavelength during 2 irradiation and recovery periods at room-temperature (IR guide 1 from le Verre Fluoré)

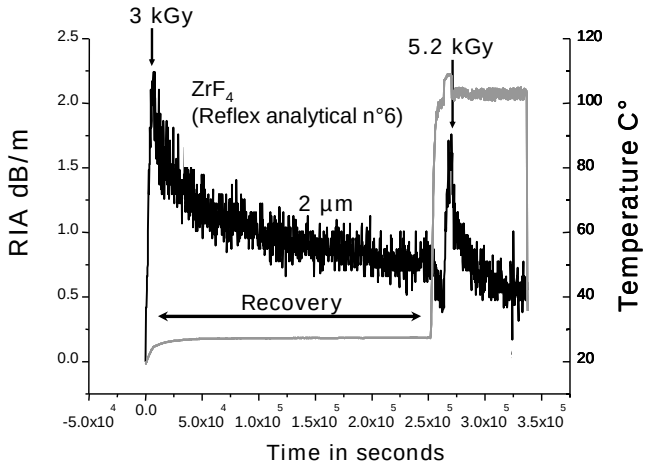

Figure 3: Effect of thermal treatment at 100°C on recovery of RIA (Reflex Analytical fibre n° 6)

The hollow waveguide fibres were irradiated at the same dose-rate but up to 25 kGy. According to the manufacturer the transmission values of these fibres at the moment of production were typically about 1 dB/m but we could only find values around 5 dB/m with our equipment described above comparing the transmission of 2 m and 8 m samples. At a test length of 2 m we did not observe a significant change in the optical transmission due to the irradiation. For a fibre of 8 m length we observed about 50% transmission loss for the same dose. The absolute values of these results have to be regarded as preliminary due to the fact that these measurements could not be performed in the online fashion due to the low overall transmission of the available samples. Nevertheless it can be stated that the hollow fibres are more robust against degradation by γ-radiation than the ZrF_4 fibres. Their high intrinsic absorption and strong sensitivity regarding the bending radius remain however a problem. For the time being, we conclude that ZrF_4 fibres could be used in the 3-4 µm region if the radiation flux does not exceed 1 Gy/s and if the fibre is simultaneously heated around 100°C. For wavelength above 3 µm, hollow fibres appear to be better candidates but only for short fibre lengths. The doses to which the fibres have been tested so far are much smaller than the full lifetime doses of ITER. The next fibres that shall be tested are sapphire fibres.

CONCLUSIONS

The results of the irradiation hardness test of the fibres seem to have ruled out the use of ZrF_4 fibres close to the divertor of ITER. The judgement on the hollow fibres is still reserved and needs further evaluation. We have however – based on the reputation of bulk sapphire [5] - some hope regarding the next tests foreseen with sapphire fibres. These results have been presented at the PSI conference in Hefei, China [6].

After these first experiments the experimental setup needed some repair and the scheduling of subsequent experiments shifted to 2007. For this second series of exposures to γ-irradiation we bought a 2 m long sapphire fibre of 250 µm core diameter. The initial transmission measurements before irradiation performed with the repaired equipment showed in comparison with a ZrF_4 fibre – as was to be expected - a smaller useful transmission range – up to about 2.8 µm. The start of the irradiation test of this fibre is the 22nd of January 2007.

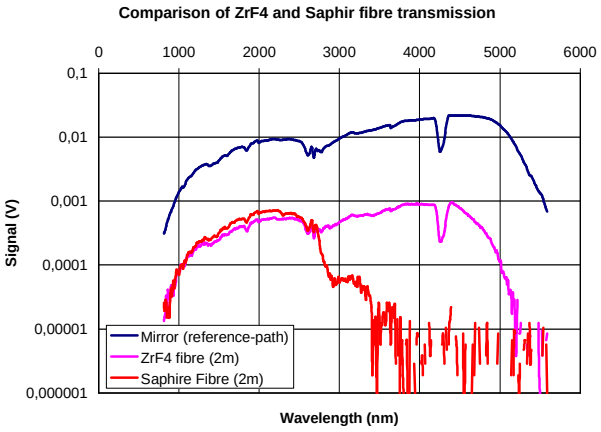

Figure 4: Signal strength mesured in experimental setup without inserted fibre (reference-path) and with ZrF_4 and sapphire fibre inserted in the measurement path

REFERENCES

[1] R.Reichle et al., Proc. 32nd EPS Conf. on Plasma Phys., ECA Vol. 29C P4.083 (2005)

[2] R. Reichle, et al., J. Nucl. Mater. 313-316, (2003) 711

[3] J. A Harington, United States Patent, Number 5,815,627 Date: Sep 29 1998

[4] A.E. Costley et al., Fusion Engineering and Design 55 (2001) 331-346

[5] E. Colby et al., IEEE Transact. Nucl. Science, 49 (2002), 2857

[6] R. Reichle et al., contr. 17 Int. Conf . Plasma Surface Interactions in Contr. Fusion Devices, Heifei, China, 22-26 May 2006, to be publ. In Journ. Nucl. Mat. 2007

TASK LEADER

Roger REICHLE

DSM/DRFC/SIPP/GID
CEA-Cadarache
F-13108 Saint-Paul-lez-Durance Cedex

Tel. : 33 4 42 25 63 76
Fax : 33 4 42 25 49 90

e-mail : roger.reichle@cea.fr

TW6-TPDS-DIADEV-D03a

Task Title: EFFECTS OF RF-HEATING ON THE MEASUREMENT CAPABILITY OF NEUTRON CAMERAS AND ALPHA PARTICLE DIAGNOSTICS

INTRODUCTION

The objective of the task is to investigate the effect of fast ions generated by auxiliary heating on ITER diagnostics. In particular, existing simulation codes for Ion Cyclotron Resonance Frequency (ICRF) and Neutral Beam Injection (NBI) are exploited for this purpose. There are essentially two issues to be considered: (i) the capability of planned ITER diagnostics to measure quantities associated with fast ions due to auxiliary heating; (ii) the interference of such ions with measurements aimed at diagnosing fusion alpha particles. As an example of the former, one can mention the question of asymmetries in the neutron emission profile. Owing to the fact that fast ions generated by auxiliary heating almost always have an anisotropic velocity space distribution; their density can vary along a flux surface. Moreover, since they are frequently one of the fuel ion species, this would lead to a poloidally varying neutron emission. In order to measure such effects a vertical neutron camera is needed in addition to a horizontal one. However, it is first necessary to assess if the effect is expected to be strong enough to be detectible. One of the subtasks is to investigate this issue. The Collective Thomson Scattering diagnostic can be used to illustrate the second question. This kind of instrument measures the velocity distribution of fast ions at points in space where a probing beam intersects a diagnostic one. However, for a given velocity of the fast ions the instrument cannot discriminate between signals coming from fusion alpha particles and other fast ions with the same velocity. Since NBI will use deuterons with an initial energy of 1MeV and ICRF heating is expected to generate fast ions in the MeV range, a significant part of the alpha particle velocity range will overlap with that of fast ions from auxiliary heating sources. It is therefore important to predict the relative abundance of alpha particles and fast ions generated by auxiliary heating.

The task started in October 2006, and only starts up activities were undertaken during 2006. In addition to carry out simulations of ICRF heated ITER discharges, the author of the present report has also been asked to coordinate the overall activity.

2006 ACTIVITIES

KICK-OFF MEETING DECEMBER 2006

In order to start up the work on the task a “kick-off” meeting was organised at the JET on the 1st of December 2006. It was possible to take advantage of the fact that many of the interested parties were at JET, for the experimental campaign, to have a largely face to face meeting, with only a few remote participants. In particular, representatives from four simulation codes and four different diagnostic techniques were took part.

The December meeting was devoted to exploring the ITER scenarios which one should prioritize in the simulation campaign. Moreover, the detailed requirements from the diagnostic experts on the quantities to be simulated were discussed at some length. This was aided by presentations detailing the diagnostic techniques. A review of the capabilities of the simulation codes was also started at the meeting, and completed at a subsequent meeting held in January 2007. As a result, the scenarios and the quantities that should be simulated during the execution of the main part of the task in 2007 were decided.

Leading up to the meeting, work was carried out on identifying relevant ITER scenarios, preparing presentations and organisational issues. Below follows a summary of the discussions and conclusions from the meeting, which have established a firm basis for the main simulation and analysis work to be carried during 2007.

ITER SCENARIOS

There are no “official” ITER scenarios available yet. However, a number of scenarios have been simulated by Polevoi et al. from the ITER CTA with the ASTRA code, see [1]. The results of these simulations can be found on the website for scenarios maintained by Gabriella Saibene [http://efdasql.ipp.mpg.de/saibene/ITER_Eq_Restricted/equilibria_index.htm]. In particular, one can find results for the three most important scenarios: standard H-mode, the hybrid scenario, and the steady state scenario (with an ITB). In terms of characteristic parameters (q-profile, temperature, density etc.), the difference is greatest between the standard H-mode and the steady state scenario, see e.g. figure 1 which shows the q-profiles of the different scenarios. It has therefore been agreed that the priority is to simulate the standard H-mode scenario and the steady state scenario.

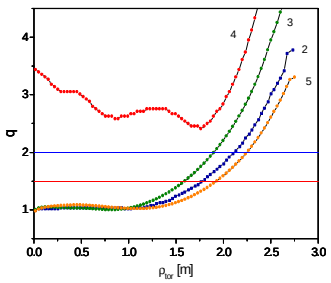

Figure 1: q-profiles for different inter scenarios: (2) standard H-mode, (3) hybrid scenario; (4) steady state scenario (ITB)

It should be noted that many of the effects that could be of interest would be more pronounced during the start-up phase of an ITER plasma than during the more stationary phase. It might therefore be necessary to make some simulations at lower temperature and densities than can be found in the simulations mentioned above.

It is also necessary to consider the heating scenarios to simulate. In the case of NBI, this is quite straight forward. The total NBI power planned for ITER is 33MW; the injected species is deuterium, and the injection energy is 1MeV. The injection geometry can be found in [http://www.iter.org].

The situation regarding ICRF heating is a little more complicated. The frequency range planned for ITER allows for four different ICRF scenarios, see the table 1.

Table 1: Frequency range for ITER scenarios

Resonance	Frequency (MHz)	Comment
$\omega=2\omega_{cT}$	53	Main scenario, the second harmonic T absorption can be combined with ^{3}He minority absorption to increase ion heating fraction in the start-up phase of an ITER plasma
$\omega=2\omega_{cD}$	50	Minority D heating; tritium rich plasma; parasitic absorption by alpha particles and Be
FWCD	56	Fast Wave Current Drive, little fast ion production.
$\omega=\omega_{cHe\text{-}3}$	45	Minority current drive near the q = 1 surface, modest fast ion population.

The D minority scenario is of somewhat limited interest since it requires a tritium rich plasma. Moreover, there can be significant parasitic absorption by fusion born alpha particles and Beryllium impurities. The FWCD scenario should not produce any significant fast ion population (most of the power should be absorbed by the electrons), and we need not be concerned with it for the present task. Minority current drive with ^{3}He minority should not produce a significant population of fast ions either. The resonance is far off-axis leading to a relatively low power density (the volume in which the power is absorbed is larger as compared to on-axis absorption). Thus, for the present assessment, the ^{3}He minority current drive scenario is not a priority. This leaves us with the main heating scenario, second harmonic tritium, around which the efforts should be concentrated. An advantage here is that NBI injected species is different from the main ICRF heated species. This implies that the simulations of ICRF and NBI can be carried out independently. It should, however, be noted that owing to the significant Doppler broadening for D injection at 1MeV, there can be some parasitic absorption on the injected deuterium ions during second harmonic tritium heating. The effect should be small, and will be neglected during the initial assessment. If time allows, one could try to quantify the effect in more detail.

In view of the above considerations, it has been decided that the ICRF simulation work should concentrate on the second harmonic tritium scenario. Since in the start up phase of an ITER plasma the introduction of a ^{3}He minority (2-3%) can be used improve the ion heating fraction in this scenario. the simulations should be carried out with different ^{3}He concentrations. Moreover, moderate variations of the resonance position should be considered.

ICRF SIMULATION CODES

The simulation effort carried out at CEA-Cadarache is concentrated on ICRF heating. A brief description of the PION and SELFO codes is therefore given here; this will also facilitate the understanding of the quantities and cases that can be simulated by the codes.

PION code

The PION code [2] was developed at JET during the late eighties and early nineties, in response to demands for simulation results that could be compared to measured quantities on a routine basis. At the time there was not enough computing power available to allow for routine analysis using a combination of the then most comprehensive codes (Full wave for power the deposition and 2D bounce averaged Fokker-Planck for the distribution function(s) of the resonating ions). Instead, it was necessary to use simplified models.

The power deposition in PION uses the model developed by Hellsten and Villard [3]. It based on fundamental observations of the behaviour of the wave field in a toroidal device. In sense one could say that the model parameterizes the results of a full wave code. The model is robust, but it has limitations. In the present context, it should be noted that it provides the flux surface average power deposition profile only, i.e. the absorption cannot be poloidally resolved.

In order to reduce the computing time and to ensure good convergence for the high power densities typical of JET, the Fokker-Planck equation is reduced to 1D by averaging over the pitch angle. The pitch angle averaged distribution is sufficient to calculate many of the most important moments normally needed (fast ion energy content, collisional power transfer to the background plasma, neutron rates etc.). However, some information on the anisotropy is also needed. Such information is obtained from a model of the anisotropy, which has been benchmarked with a 2D bounce averaged code. Consequently, it is possible to calculate profiles of the parallel and perpendicular energy density of the resonating ions (and of course also the pressure), the density of fast ions on a flux surface and their effective perpendicular and parallel temperatures. However, poloidally resolved quantities cannot be obtained.

Finite orbit width effects often play an important role; a simplified method to account for this is employed in PION. It is based on the observation that fast ICRF accelerated ions tend to pile up with their turning points near the cyclotron resonance, collisions coefficients are therefore averaged over such orbits, and they are also used to redistribute the collisions power to the background ions and electrons etc.

The simulation of ICRF heating is complicated by the fact that the two problems, power deposition and distribution function calculations, are dependent on each other, which necessitates self-consistent simulations. In order to address this problem, the PION code produces output used in the power deposition calculation to modify the dielectric tensor contributions from the resonating ions. In particular, this procedure ensures that the absorption strength is consistent in the two calculations, which is important for the partition of the power between different species.

The PION code is run in the secondary processing chain in JET (CAHIN 2), and is still one of the few ICRF codes that can be used for routine analysis. It has been extensively benchmarked against JET results, see for instance results from the JET DT campaign in 1997 [4].

The SELFO code

The SELFO code [5] [6] combines the full wave code LION [7] with the Fokker-Planck code FIDO [8]. The latter solves a 3D orbit averaged Fokker-Planck equation for the resonating ions with a Monte-Carlo method (see e.g. [9].) All effects of wave induced velocity space and spatial transport are taken into account. Moreover, the code handles the finite width of guiding centre orbits; including non-standard orbits in the potato regime (see e.g. [10]).
A limitation in the present version of the FIDO code is the assumption of circular flux surfaces. However, for the purposes of the assessment needed for the present task this is not a major issue. Furthermore, there are some limitations of the power deposition calculation which, like PION, cannot handle cases with significant mode conversion (conversion of the launched fast wave to short wave length modes near cyclotron resonances). Since the ITER scenarios to be considered should have very modest amounts of mode conversion, this limitation will not pose any problems.

The SELFO code follows the temporal evolution of the ICRF power deposition and the distribution function(s) of the resonating ions. The results from the FIDO code are used to calculate the contribution form the resonating ions to the dielectric tensor in each point in space; the new dielectric tensor is then used in the LION code to calculate the wave field/ power deposition for the nest time step. Thus, SELFO code (like PION) provides a self consistent solution of the ICRF power deposition and the distribution function(s) of the resonating ions.

The SELFO code can provide a poloidally resolved distribution functions. However, since a Monte Carlo method is used, the moments of the distribution function are better represented than the function itself (more Monte Carlo test particles, i.e better statistics, are necessary to have a decent representation of the distribution itself). Thus, the SELFO code is suitable for providing poloidally resolved moments of the distribution function, like neutron rates. Furthermore, the distribution function can be reconstructed at every point in space provided a sufficient number of Monte Carlo test particles are used; it is not foreseen to make many runs of this kind.

The SELFO code has been benchmarked against JET discharges, especially in connection with the wave induced spatial transport in the presence of asymmetrically lunched toroidal mode spectra [11] [12].

IMPACT OF FAST IONS GENERATED AUXILIARY HEATING ON ITER DIAGNOSTICS – MAIN AREAS OF INVESTIGATION

In this section the main impact on fast ions on the different diagnostics is discussed. Moreover, an assessment is made of the quantities that need to be simulated.

Alpha Knock-on Neutron measurements with additional plasma heating in ITER

The main issue here concerns the ability to measure knock-on tails due to alpha particles in the presence of auxiliary heating in ITER. Knock-on neutrons is the result of a fast ion, e.g. an alpha particle, having a close collision with a thermal fuel ion; as a result, the latter acquires a high velocity (significantly higher than the thermal), reactions between a non-thermal population of fuel ions due to knock-on collisions and thermal fuel ions give rise to knock-on neutrons. The signature of these is a tail in the neutron spectrum, see figure 6. Obviously, the tail due to the knock-on reactions of alpha particles can be masked by a tail on the distribution function of one of the fuel species due to auxiliary heating. Moreover, a non-thermal tail on a fuel species can in itself give rise to knock-on reactions. Consequently, it is important to simulate the effect of the distortion caused by auxiliary heating on the distribution functions of fuel ion species.

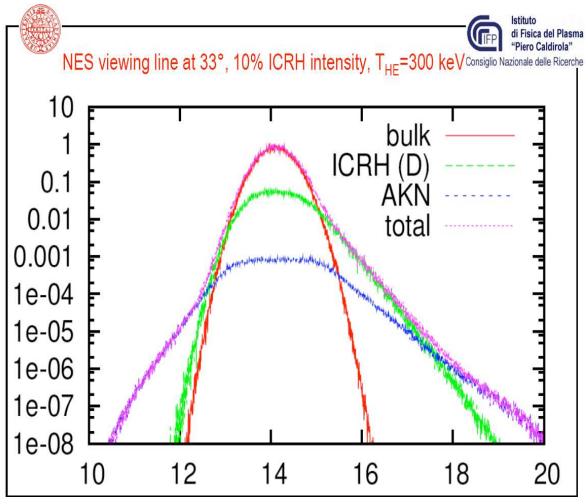

Figure 6: Example of simulated neutron spectrum with alpha knock on reactions and a tail of tritons with an assumed non-thermal Maxwellian distribution having a equivalent temperature of 300 keV

Ideally the diagnosticians would like a 4D distribution function, $f(R, Z, v_{\parallel}, v_{\perp})$, of the fuel ion species' distribution function in the presence of auxiliary heating (they can plug them directly in to existing analysis codes for the knock-on spectra). While it is possible to produce 4D distribution functions, it is not optimal for the simulation codes based on the Monte-Carlo method. The statistics tend to be poor in the tail of the test particle distribution function. In the case of NBI distorted tails, it should be relatively straightforward to produce the 4D

distribution function even with a Monte-Carlo code. It is a more challenging problem for ICRF distorted distribution functions, but it is nevertheless possible if a sufficient number of Monte-Carlo Test particles is used. Thus, the runs for ICRF heated ions will be fairly long, and only a very limited number can therefore be carried out. On the other hand, the model with an ad hoc tail temperature used so far for the simulations of the knock-on spectra in the presence of ICRF heating can be improved upon. In particular, one can use the PION code to produce realistic densities and averaged energies of the ICRF heated distribution functions. Since PION can be used for routine analysis this should provide a good guidance regarding the sensitivity of the measurements to various quantities (like resonance position, concentration of ^{3}He ions etc.).

Consequently, in order to explore the parameter space, the PION code will be used. The output of flux surface averaged perpendicular and parallel tail temperatures together with the density of fast ions will be used to assess the impact on the knock-on tail formation. The information from the PION code will be communicated to the diagnosticians who will use it in their simulation codes.

In a small number of cases, comprehensive SELFO runs, which reconstruct the velocity distribution locally in space, will be used for more detailed assessments. The distribution function will be communicated to the diagnosticians for use in their simulation codes.

2D neutron emissivity profiles in the of NBI and ICRF heating

As discussed in the introduction, an important question is wether there will be a significant asymmetry (along a flux surface) in the neutron emission during NBI and/or ICRF heating in ITER. The motivation for having a vertical neutron camera hinges on it. In order to investigate this, the neutron emission profile must be computed for each position in the plasma. It involves evaluating the following integral:

$$S(R,Z) = n_D n_T \langle \sigma \mathrm{v} \rangle_{DT}$$

$$\langle \sigma v \rangle_{DT} = \int\int f_D(\vec{\mathrm{v}}_D) f_T(\vec{\mathrm{v}}_T) \sigma(|\vec{\mathrm{v}}_D - \vec{\mathrm{v}}_T|) \, |\vec{\mathrm{v}}_D - \vec{\mathrm{v}}_T| \, d\vec{\mathrm{v}}_D d\vec{\mathrm{v}}_\mathrm{T}$$

The emission profile, poloidally resolved, is probably most easily calculated as an output from the NBI and ICRF simulation codes, rather than transferring a distribution function to a code evaluating the above integral separately. The only problem is if one distribution is taken from a code simulating an ICRF distorted distribution function (e.g. second harmonic T) and the second from another code simulating the neutral beam fast ion distribution function (D injection).

As a first approximation it will be assumed that one of the reacting species has a Maxwellian distribution function, i.e. the non-thermal – non-thermal reactions will be neglected. Consequently, the polodally resolved emission profile will be calculated separately from NBI and ICRF simulation codes. Only if there is perceived need at a later stage should the possibility of combining a NBI non-thermal distribution with an ICRF distorted one be considered.

Assessment of gamma-ray measurement capabilities

The main point of this investigation is to assess the 2D gamma-ray (poloidally resolved) emission resulting from interaction of non-thermal ions, caused by auxiliary heating, and impurities in the plasma (mainly Carbon and Beryllium). This is again of importance for the justification of the vertical neutron camera. However, this study has a more general interest: assessing the capabilities of using gamma rays to diagnose fast ions in ITER.

The relevant cross sections will be worked out by Vasili Kiptily. They will then be implemented in the different codes. In order to simulate the gamma-ray spectra for ICRF heated ions both the PION and SELFO can be used, with the latter being employed to simulate the poloidally resolved emission for a small number of cases.

Fast ion CTS for ITER

A critical point of the proposed Collective Thomson Scattering diagnostic is that it does not make any distinction between different species of fast ions, i.e. for a given velocity it is not possible to say which species give rise to the measured signal.
Thus, if one wants to obtain information on the projection of the alpha particle distribution function

$$g_\alpha(u) = \int f_\alpha(v) \delta(v \cdot \hat{k} - u) dv$$

in the intersection region of the CTS probe and receiver beams, the corresponding g_s(u) for other fast ion species must be much smaller than g_alpha(u). Here *k* is the resolved direction defined by the scattering geometry. This information can relatively easily be obtained from the simulation codes for the auxiliary heating. Essentially it is a question of calculating the distribution function at a point in the plasma where the two beams intersect. For more accurate simulations one could average over the finite area consistent with the widths of the beams, but this is probably beyond the scope of the initial assessment.

A rough assessment of the impact of ICRF heated fast ions on the CTS diagnostic for different parameters can be made with the PION code. Essentially it is a question of comparing the projected alpha particle distribution function, g(u), with that of the ICRF accelerated fast ions for a given u = v*k, where * is the vector dot product. For a small number of cases where the tails of the ICRF accelerated fast ions are of the same order as that of the alpha particles, SELFO simulations will be used. In the SELFO code, the velocity distribution function should be reconstructed in the region where the probing CTS beam intersects the diagnostic one. What can be of special interest here is the anisotropy of the distribution function of the ICRF heated ions.

A rough assessment of the impact of ICRF heated fast ions on CTS diagnostic for different parameters can be made with the PION code. Essentially it is a question of

comparing the alpha particle distribution function with that of the ICRF accelerated fast ions for a given velocity.
For a small number of cases where the tails of the ICRF accelerated fast ions are of the same order as that of the alpha particles, SELFO simulations will be used. In the SELFO code, the velocity distribution function should be reconstructed in the region where the probing CTS beam intersects the diagnostic one. What can be of special interest here is the anisotropy of the distribution function of the ICRF heated ions.

CONCLUSIONS

The work on the task has started up well during 2006. In particular, the ITER scenarios which should be simulated as a matter of priority have been decided. Furthermore, a detailed review has been made of the quantities that should be simulated in order to address the most pertinent issues regarding the influence of fast ions generated by auxiliary heating on ITER diagnostics.

REFERENCES

[1] Polevoi et al., J. Plasma Fusion Res. SERIES 5, 82 (2002)

[2] L.-G. Eriksson, T. Hellsten and U. Willén, Nuclear Fusion 33 (1993) 1037

[3] T. Hellsten and L. Villard, Nuclear Fusion 28, 285 (1998)

[4] L.-G. Eriksson, M. Mantsinen et al., Nuclear Fusion 39, 337 (1999)

[5] J. Hedin, T. Hellsten, J. Carlsson, Proc. of Joint Varenna-Lausanne Workshop on “Theory of fusion Plasmas” 467, Varenna (1998);

[6] J. Hedin et al., Nuclear Fusion 42, 527 (2002)

[7] Villard et al., Computer Physics Reports 4, 95 (1986)

[8] J. Carlsson, T. Hellsten and L.-G. Eriksson, In proceedings of “Theory of Fusion Plasmas”, Joint Varenna-Lausanne International Wokshop, 1994

[9] L.-G.Erikson and P.Helander, Physics of Plasmas 1, 308 (1994)

[10] L.-G. Erikson and F Porcelle, Plasma Physics and Controlled Fusion 43, R145 (2001)

[11] T. Johnsson et al, IAEA Technical Meeting on “Fast Particles in Fusion Plasmas”, Gothenburg, 2001

[12] Mantsinen et al., Physical Review Letters 91, 115004 (2002)

TASK LEADER

Lars-Göran ERIKSSON

DSM/DRFC/SCCP/GSEM
CEA-Cadarache
F-13108 Saint-Paul-lez-Durance Cedex

Tel. : 33 4 42 25 49 40
Fax : 33 4 42 25 62 33

e-mail : lars-goran.eriksson@cea.fr

CEFDA06-1376

Task Title: TW5-TPR-RPSUP: SUPPORT TO EFDA REMOTE PARTICIPATION

INTRODUCTION

The main objective of this Task is to co-ordinate the Remote Participation (RP) activity in the EFDA Technology Workprogramme. The RP activity aims at enhancing the capabilities for remote computer and data access, teleconferencing and distributed computer design tools within all the Euratom Fusion Associations and the EU ITER Participant Team (PT) design and R&D studies.

2006 ACTIVITIES

We organised a technical RP workshop for technical contact persons. This workshop took place on 20/21 June 2006 in RIGA (Latvia). Its main objectives were to review the existing remote participation technologies and to establish a work and development program for 2006/2007. We counted almost 40 participants, among them 14 were remote, from 22 EFDA labs in 16 countries.

In order to facilitate the communication between the technical contacts we developed and launched in November 2006 a wiki site for EFDA RP. This site is a url accessible via https. It is hosted and managed by DRFC. It is based on XWiki technology http://www.xwiki.org.
It is a common repository, accessible without any former knowledge to every technical contact person, either to consult information, or to put new information for the community, articles, documents or links, and also to discuss and comment the news.
It is organized according to the principal RP themes. It got page editing, version control, rights management, full-text search, its access is restricted to authorized people and it is moderated. It is totally programmable so it would fit at term all user's needs and demands. It is available from any browser and rss feeds can be used to be warned about new contributions.

A meeting on authentication and authorisation systems, especially on PAPI and shibboleth systems took place at JET on 28th November, 2006. In conclusion the meeting agreed that PAPI based federation will be set up for web access as a test bed. The participants are CIEMAT, CEA, JET, KFKI/HAS, EFDA, where JET offers the middle-tier of users page, KFKI the EFDA RP videoconference archive in cooperation with NIIF/Hungarnet, EFDA offers its web site and possible would undertake the role as GPoA if resources allow it.
It was also discussed that other EFDA labs will be also asked for their interest in a federated management of internal Websites.

As decided during the workshop in Riga, we would participate to regular videoconference the first Wednesday of the month every two months. These conferences are dedicated to the progress and issues of videoconference. The conference allows by itself to measure and comment what works well and the possible problems that sometimes occur.

We participate to the collection of information from technical contacts for a set of surveys, asked by the EFDA leader, Jerome Pamela, and concerning the various part of remote participation activity, remote computer and data access, network issues, teleconferencing and remote experimentation. The results are presently being compiled and will be soon available on the wiki site.

CONCLUSIONS

Coordination of remote participation activity among European labs is a long term task. The best improvements have been noticed in videoconferencing with the generalisation of the H323 standard.

REPORTS AND PUBLICATIONS

- Deliverable D1 : Report on Major Review Workshop RPTC-0193 September 2006

TASK LEADER

Stéphane BALME

DSM/DRFC/STEP/GDPI
CEA-Cadarache
F-13108 Saint-Paul-Lez-Durance Cedex

Tel. : 33 4 42 25 47 48
Fax : 33 4 42 25 26 61

e-mail : stephane.balme@cea.fr